

Interference in Spectrum-Sharing Integrated Terrestrial and Satellite Networks: Modeling, Approximation, and Robust Transmit Beamforming

Wenjing Cao, Yafei Wang, *Graduate Student Member, IEEE*, Tianxiang Ji, Tianyang Cao, Wenjin Wang, *Member, IEEE*, Symeon Chatzinotas, *Fellow, IEEE*, Björn Ottersten, *Fellow, IEEE*

Abstract—This paper investigates robust transmit (TX) beamforming from the satellite to user terminals (UTs), based on statistical channel state information (CSI). The proposed design specifically targets the mitigation of satellite-to-terrestrial interference in spectrum-sharing integrated terrestrial and satellite networks. By leveraging the distribution information of terrestrial UTs, we first establish an interference model from the satellite to terrestrial systems without shared CSI. Based on this, robust TX beamforming schemes are developed under both the interference threshold and the power budget. Two optimization criteria are considered: satellite weighted sum rate maximization and mean square error minimization. The former achieves a superior achievable rate performance through an iterative optimization framework, whereas the latter enables a low-complexity closed-form solution at the expense of reduced rate, with interference constraints satisfied via a bisection method. To avoid complex integral calculations and the dependence on user distribution information in inter-system interference evaluations, we propose a terrestrial base station position-aided approximation method, and the approximation errors are subsequently analyzed. Numerical simulations validate the effectiveness of our proposed schemes.

Index Terms—Spectrum-sharing, integrated terrestrial and satellite networks, TX beamforming, statistical CSI, position-aided approximation.

I. INTRODUCTION

SATELLITE communications are crucial for enabling ubiquitous connectivity in the 6th generation (6G), playing a significant role in achieving broad coverage across space, air, ground, and sea [1], [2]. However, the competition for spectrum among various wireless communication systems has intensified, especially in frequency bands below 6 GHz [3]–[5], posing significant challenges to the allocation of dedicated frequencies for satellite communications. Spectrum sharing in integrated terrestrial and satellite networks (ITSNs) has emerged as a promising solution [6]–[12], allowing satellites and terrestrial communication networks to utilize the same spectrum to enhance spectrum efficiency, as demonstrated by early efforts such as cognitive radio for satellite

communications (CoRaSat) technology [13], [14] and shared access terrestrial-satellite backhaul network enabled by smart antennas (SANSA) project [15], [16]. However, the overlap of the operating spectrum between terrestrial and satellite systems may cause inter-system interference within their overlapping coverage areas, leading to degradation in overall system performance [17]–[19]. In sub-6GHz ITSN scenarios, where satellite communications is considered complementary to terrestrial mobile networks, satellite user terminals (UTs) are often located outside the coverage of terrestrial base stations (BSs), making interference from BSs to satellite UTs negligible [20], [21]. Nevertheless, due to the broader coverage of satellite beams [22], interference from satellites to terrestrial UTs may still occur at the interface of the two systems. Therefore, mitigating interference between terrestrial and satellite systems is essential for efficient spectrum sharing of ITSNs.

Transmit (TX) beamforming is widely recognized as an effective technique for interference management in satellite communication systems [23], [24]. Studies in CoRaSat and SANSA primarily focused on high-frequency bands (e.g., Ka and Ku bands) and geostationary earth orbit satellites, while recent developments have shifted interest toward spectrum sharing in sub-6GHz bands and low earth orbit (LEO) satellites [25], driven by direct-to-cell satellite initiatives such as AST SpaceMobile’s BlueWalker 3 and SpaceX’s Starlink V2 Mini [26]. Benefiting from their extremely large antenna arrays onboard, these satellites enable advanced beamforming capabilities [27]. Conventional TX beamforming methods, such as maximum ratio transmission (MRT) beamforming, zero-forcing (ZF) beamforming, minimum mean square error (MMSE) beamforming, weighted MMSE (WMMSE) beamforming, total power minimization beamforming, and energy efficiency beamforming [28]–[33], require perfect instantaneous channel state information (iCSI) to achieve optimal performance. However, due to the long satellite-to-terrestrial distance and the high mobility of satellites, obtaining accurate iCSI is challenging, and beamforming design based on statistical CSI (sCSI), e.g., the angle of departure (AoD), becomes a more practical approach. For example, a beamforming method based on sCSI, including angle and power information, was proposed in [20] with the objective of maximizing the average signal-to-interference-plus-noise ratio (SINR). To against errors in the AoD within sCSI, [34] proposed a robust beamforming scheme with a more practical per-antenna power

Manuscript received xxx; revised xxx.

Wenjing Cao, Yafei Wang, and Wenjin Wang are with the National Mobile Communications Research Laboratory, Southeast University, Nanjing 210096, China, and also with Purple Mountain Laboratories, Nanjing 211100, China (e-mail: caowj@seu.edu.cn; wangyf@seu.edu.cn; wangwj@seu.edu.cn).

Tianxiang Ji and Tianyang Cao are with China Mobile Group Design Institute Company Ltd., Beijing 100089, China (e-mail: jitianxiang@cmdi.chinamobile.com; caotianyang@cmdi.chinamobile.com).

Symeon Chatzinotas and Björn Ottersten are with the Interdisciplinary Centre for Security, Reliability and Trust (SnT), University of Luxembourg, Luxembourg (e-mail: symeon.chatzinotas@uni.lu; bjorn.ottersten@uni.lu).

constraint.

Although the aforementioned TX beamforming schemes effectively mitigate intra-system user interference, they cannot be directly applied to ITSN systems, as they do not consider inter-system interference. To address this challenge, some works have proposed dedicated TX beamforming designs to handle inter-system interference. To eliminate interference from terrestrial BSs to satellite UTs, [35] proposed a TX beamforming method at the terrestrial BS side under the minimum user rate constraint, and this terrestrial interference was further restricted to an interference power threshold in [36], [37]. Joint TX beamforming design for terrestrial and non-terrestrial systems based on shared CSI is another research avenue for interference management. [8], [38] proposed joint TX beamforming designs subject to minimum user rate constraints, while [39] optimized joint beamforming to meet the minimum SINR for each UT in ITSNs. In sub-6GHz ITSNs, where the terrestrial system serves as the primary network and interference from BSs to satellite UTs is negligible [20], [21], mitigating satellite-to-terrestrial interference becomes a more practical and relevant concern. To reduce satellite interference, [40] proposed a TX beamforming design with cloud-based CSI and introduced an interference threshold for terrestrial UTs, with the objective of maximizing the satellite UT rate. In [41], the TX beamforming leveraged shared CSI to mitigate satellite interference while constraining a minimum rate for each terrestrial UT. Compared to joint satellite-terrestrial beamforming designs, optimizing TX beamforming solely on the satellite side significantly reduces complexity due to the lower optimization dimensions.

Most existing TX beamforming schemes for ITSNs rely on CSI sharing between the satellite and the terrestrial system [39]–[43], which incurs substantial additional communication overhead and suffers from CSI delay due to mobility. However, CSI sharing in ITSNs poses significant challenges for current system architectures due to the lack of protocol support for shared CSI transmission and the large volume of real-time CSI data from terrestrial UTs, which requires collaboration between terrestrial and satellite operators [44]. Thus, a key question arises: *How to design robust TX beamforming without shared CSI against satellite-to-terrestrial interference in ITSNs?* This is the central issue to be investigated in this paper. In summary, our principal contributions are as follows:

- To address the challenge of CSI sharing in ITSNs, we develop an integral-form interference model free of shared CSI for the satellite downlink. This model targets the interference from the satellite to terrestrial UTs. Specifically, we derive the interference power as an integral expression, utilizing prior knowledge of the corresponding BS positions and the distribution of terrestrial users. Thus, this interference model eliminates the dependence on CSI sharing in ITSNs.
- Based on the proposed interference model and statistical CSI, we design robust satellite TX beamforming schemes for interference mitigation in ITSNs. The weighted sum rate (WSR) maximization problem for the satellite is formulated under the interference threshold and power budget, and solved iteratively by transforming the frac-

tional objective into a convex form using multidimensional complex quadratic transformation (MCQT). To reduce complexity, we reformulate the problem as an equivalent WMMSE problem and derive the closed-form beamforming matrix for iteration from the Karush-Kuhn-Tucker (KKT) conditions.

- To further simplify the design, we propose a low-complexity and robust satellite TX beamforming scheme. We derive the MMSE problem for the satellite under the interference and power constraints, obtain the optimal closed-form solution, and apply a bisection method to satisfy the interference threshold for terrestrial UTs. This scheme avoids high-dimensional iterative updates, offering a favorable trade-off between performance and computational efficiency.
- We propose an interference approximation scheme that uses terrestrial BS position information to approximate the integral-form interference term. This scheme reduces the complexity of interference integral calculations and the challenge of obtaining real-time user distributions. Furthermore, we analyze the key factors affecting the approximation error, providing guidance for the utilization of this approximation.

The rest of the article is organized as follows: The system model is established in Section II. The WSR beamforming problem and the corresponding schemes are investigated in Section III. The MMSE beamforming problem and its closed-form solution are derived in Section IV. In Section V, we propose an interference approximation scheme and analyze the approximation error. Simulation results are provided in Section VI, and Section VII concludes this article.

Notation: $x, \mathbf{x}, \mathbf{X}$ represent scalar, column vector, matrix. $(\cdot)^T, (\cdot)^*, (\cdot)^H$, and $(\cdot)^{-1}$ respectively denote the transpose, conjugate, transpose-conjugate, and inverse operations. $\|\cdot\|_2$ denotes l_2 -norm. $\|\cdot\|_F^2$ denotes frobenius norm. \otimes is the Kronecker product operation. The operator $\text{Tr}\{\cdot\}$ represents the matrix trace. $\mathbb{E}\{\cdot\}$ denotes the expectation. $\text{diag}\{\mathbf{a}\}$ represents the diagonal matrix whose diagonal elements are composed of \mathbf{a} . $[\mathbf{X}]_{i,j}$ denotes the (i, j) -th element of \mathbf{x} . The expression $\mathcal{CN}(\mu, \sigma^2)$ denotes circularly symmetric Gaussian distribution with expectation μ and variance σ^2 . $\mathbb{R}^{M \times N}$ and $\mathbb{C}^{M \times N}$ represent the set of $M \times N$ dimension real- and complex-valued matrixes. ∇f denotes gradient of function $f(\cdot)$. $k \in \mathcal{K}$ means element k belongs to set \mathcal{K} .

II. SYSTEM MODEL

In Fig. 1, we consider a spectrum-sharing satellite downlink scenario in ITSNs, where the primary terrestrial network coexists with a secondary satellite network. A LEO satellite serves K_S satellite UTs, and N_G terrestrial BSs serve K_G terrestrial UTs. The satellite and terrestrial systems have partially overlapping coverage areas at the edges [44], within which a portion of terrestrial UTs reside. Both the terrestrial and satellite communication systems share the sub-6GHz spectrum for downlink transmission in response to the requirements of the 3rd Generation Partnership Project (3GPP) [10], [45].

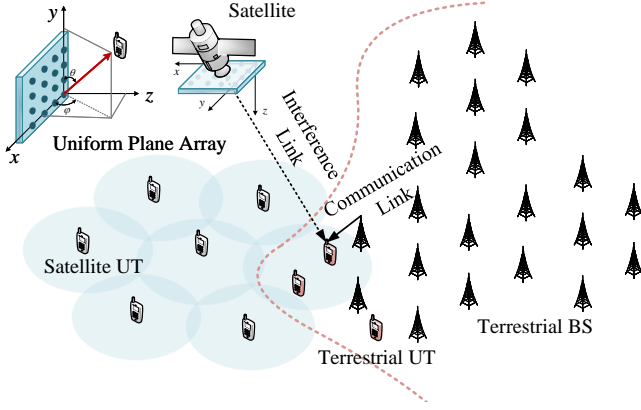


Fig. 1. The system architecture of the ITSN.

A. Channel and Signal Model

We consider a satellite equipped with a large-scale uniform planar array (UPA) composed of $M_S = M_x \times M_y$ antennas, where M_x and M_y denote the number of antenna elements along the x -axis and y -axis, respectively. Adopting a ray-tracing-based channel modeling approach, the space-domain channel vector $\mathbf{h}_{ss,k}(t, f) \in \mathbb{C}^{M_S \times 1}$ for the satellite UT k at time instant t and frequency f can be modeled as [20], [46], [47]

$$\mathbf{h}_{ss,k}(t, f) = e^{j2\pi(t v_k^{\text{sat}} - f \tau_k^{\text{min}})} g_k^{\text{ss}}(t, f) \mathbf{v}_k^{\text{ss}}, \quad (1)$$

where g_k^{ss} represents the LEO satellite downlink channel gain. Due to the line-of-sight (LoS) propagation characteristics of satellite communication, it is assumed that the channel gain $g_k^{\text{ss}}(t, f)$ follows a Rician distribution with the Rician factor κ_k and power $\mathbb{E}\{|g_k^{\text{ss}}(t, f)|^2\} = (\gamma_k^{\text{ss}})^2$. Specifically, the real and imaginary parts of g_k^{ss} are independently and identically real-valued Gaussian distributed with mean $\gamma_k^{\text{ss}} \sqrt{\frac{\kappa_k}{2(\kappa_k+1)}}$ and variance $\frac{(\gamma_k^{\text{ss}})^2}{2(\kappa_k+1)}$, respectively [34], [48]. Additionally, v_k^{sat} refers to the Doppler shift caused by the motion of the LEO satellite, and τ_k^{min} refers to the minimum propagation delay of the k -th satellite UT. The UPA TX characteristics can be represented by the vector $\mathbf{v}_k^{\text{ss}} = \mathbf{v}_k^{\text{ss}}(\vartheta_k^x) \otimes \mathbf{v}_k^{\text{ss}}(\vartheta_k^y)$. As shown in Fig. 1, the channel space angles $\vartheta_k^x = \sin \theta_k \cos \varphi_k$ and $\vartheta_k^y = \cos \theta_k$ represent the direction cosines of the UT with respect to the UPA along the x -axis and y -axis, respectively. Herein, θ_k denotes the elevation angle and φ_k denotes the azimuth angle from the satellite to the k -th satellite UT. $\mathbf{v}_k^{\text{ss}}(\vartheta_k^x)$ and $\mathbf{v}_k^{\text{ss}}(\vartheta_k^y)$ are the steering vectors in the x -axis and y -axis as follows

$$\mathbf{v}_k^{\text{ss}}(\vartheta_k^x) = \frac{1}{\sqrt{M_x}} \left[1, e^{-j\frac{2\pi}{\lambda} d_x \vartheta_k^x}, \dots, e^{-j\frac{2\pi}{\lambda} d_x (M_x-1) \vartheta_k^x} \right]^T, \quad (2)$$

$$\mathbf{v}_k^{\text{ss}}(\vartheta_k^y) = \frac{1}{\sqrt{M_y}} \left[1, e^{-j\frac{2\pi}{\lambda} d_y \vartheta_k^y}, \dots, e^{-j\frac{2\pi}{\lambda} d_y (M_y-1) \vartheta_k^y} \right]^T, \quad (3)$$

where $d_x = d_y = \frac{\lambda}{2}$ represent the distances between adjacent antenna elements along the x -axis and y -axis.

In ITSNs, the satellite and N_G terrestrial BSs share the spectrum to provide service to corresponding UTs. Since satellites typically complement terrestrial mobile communi-

cation, we assume that in the sub-6GHz ITSN scenario, the satellite switches off the coverage over areas with terrestrial connectivity and satellite UTs are usually located outside the coverage area of terrestrial BSs, making terrestrial interference to satellite UTs negligible [21], [40]. The signal $y_{s,k}$ received by the k -th satellite UT can be expressed as

$$y_{s,k} = \mathbf{h}_{ss,k}^H \sum_{i=1}^{K_S} \mathbf{p}_{s,i} x_{s,i} + n_{s,k}, \quad (4)$$

herein, $\mathbf{p}_{s,i} \in \mathbb{C}^{M_S \times 1}$ is the beamforming vector, $x_{s,i}$ is the symbol sent by the satellite to the i -th satellite UT and $n_{s,k}$ denotes the additive noise following $\mathcal{CN}(0, \sigma_k^2)$. For brevity, we combine the received signals of all satellite UTs and reformulate the signal model as

$$\mathbf{y}_s = \mathbf{H}_{ss}^H \mathbf{P} \mathbf{x}_s + \mathbf{n}_s \in \mathbb{C}^{K_S \times 1}, \quad (5)$$

where channel matrix $\mathbf{H}_{ss} = [\mathbf{h}_{ss,1}, \dots, \mathbf{h}_{ss,K_S}] \in \mathbb{C}^{M_S \times K_S}$, beamforming matrix $\mathbf{P} = [\mathbf{p}_{s,1}, \dots, \mathbf{p}_{s,K_S}] \in \mathbb{C}^{M_S \times K_S}$. Besides, $\mathbf{x}_s = [x_{s,1}, \dots, x_{s,K_S}]^T \in \mathbb{C}^{K_S \times 1}$ is the matrix of symbols sent by the satellite satisfying $\mathbb{E}\{\mathbf{x}_s \mathbf{x}_s^H\} = \mathbf{I}$.

Despite the benefits of spectrum sharing between satellite and terrestrial networks, inter-system interference could degrade system performance. Effective interference mitigation, particularly in overlapping coverage regions of ITSNs, is essential for successful spectrum sharing [10]. To simplify the analysis, we neglect the interference among terrestrial BSs and focus on the interference from the satellite to terrestrial UTs. The average interference power to each terrestrial UT can be expressed as

$$I_{\text{avg}} = \mathbb{E}_{\mathbf{x}_s} \left\{ \frac{1}{K_G} \text{Tr} \{ \mathbf{H}_{sg}^H \mathbf{P} \mathbf{x}_s \mathbf{x}_s^H \mathbf{P}^H \mathbf{H}_{sg} \} \right\} \\ = \frac{1}{K_G} \text{Tr} \{ \mathbf{P}^H \mathbf{H}_{sg} \mathbf{H}_{sg}^H \mathbf{P} \}, \quad (6)$$

where $\mathbf{H}_{sg} \in \mathbb{C}^{M_S \times K_G}$ denotes the satellite-to-terrestrial UT channel matrix based on iCSI. This interference channel is modeled as a Rician fading channel with LoS propagation, consistent with the satellite signal link, since LoS terrestrial UTs typically suffer stronger satellite interference than non-LoS ones. The interference power, governed by power flux density limits that adapt to the beam footprint, must remain below I_{thr} in accordance with 3GPP and satellite operator standards [49], [50].

B. Foundation of Beamforming in ITSNs: sCSI or CSI-Free?

Benefiting from the large-scale antenna arrays onboard the satellite, we leverage the TX beamforming technique to mitigate the interference from the satellite to terrestrial UTs. While conventional TX beamforming design typically relies on iCSI availability, acquiring precise iCSI is generally infeasible for the satellite due to the long propagation delay, large Doppler shift, and limited pilot overhead [41], [51]. Furthermore, the frequent updating of TX beamforming vectors based on iCSI of \mathbf{H}_{ss} and \mathbf{H}_{sg} presents significant challenges for satellite payload implementation. Consequently, we design robust TX beamforming utilizing the following information in ITSNs:

1) *sCSI for Intra-Satellite System Channels*: In the satellite system, sCSI for satellite UTs includes

$$\bar{\gamma}_k^{\text{ss}} \triangleq \mathbb{E}\{g_k^{\text{ss}}(t, f)\} = \gamma_k^{\text{ss}} \sqrt{\frac{\kappa_k}{2(\kappa_k + 1)}}(1 + j), \quad (7)$$

$$\mathbb{E}\{\mathbf{H}_{\text{ss}}\mathbf{H}_{\text{ss}}^H\} = \sum_{k=1}^{K_S} (\gamma_k^{\text{ss}})^2 \mathbf{v}_k^{\text{ss}} \mathbf{v}_k^{\text{ss}H}, \quad (8)$$

which are assumed to vary slowly in satellite systems [20].

2) *CSI-Free Interference Model for Inter-Satellite and Terrestrial Systems*: The average interference power can be further expressed in statistical form

$$\begin{aligned} I_{\text{avg}} &= \mathbb{E}_{\mathbf{H}_{\text{sg}}, \mathbf{x}_s} \left\{ \frac{1}{K_G} \text{Tr} \{ \mathbf{H}_{\text{sg}}^H \mathbf{P} \mathbf{x}_s \mathbf{x}_s^H \mathbf{P}^H \mathbf{H}_{\text{sg}} \} \right\} \\ &= \frac{1}{K_G} \text{Tr} \{ \mathbf{P}^H \mathbb{E} \{ \mathbf{H}_{\text{sg}} \mathbf{H}_{\text{sg}}^H \} \mathbf{P} \} \\ &= \frac{1}{K_G} \text{Tr} \{ \mathbf{P}^H \mathbf{\Upsilon}_{\text{sg}} \mathbf{P} \}, \end{aligned} \quad (9)$$

we define $\mathbf{\Upsilon}_{\text{sg}} = \mathbb{E} \{ \mathbf{H}_{\text{sg}} \mathbf{H}_{\text{sg}}^H \} = \sum_{k=1}^{K_G} (\gamma_k^{\text{sg}})^2 \mathbf{v}_{n,k}^{\text{sg}} \mathbf{v}_{n,k}^{\text{sg}H}$. Due to the numerous interfered terrestrial UTs, obtaining all of their sCSI may still incur significant. Moreover, the satellite array exhibits limited spatial resolution, making it difficult to discriminate among closely located terrestrial UTs. To address these issues, we convert the sum of the discrete terrestrial UT channels into an integral of the user distribution over the terrestrial BS coverage. The integral is given by

$$\begin{aligned} \mathbf{\Upsilon}_{\text{sg}} &= \mathbb{E} \{ \mathbf{H}_{\text{sg}} \mathbf{H}_{\text{sg}}^H \} = \sum_{n=1}^{N_G} \mathbb{E} \left\{ \sum_{k=1}^{\bar{K}_G} |g_{n,k}^{\text{sg}}(t, f)|^2 \mathbf{v}_{n,k}^{\text{sg}} \mathbf{v}_{n,k}^{\text{sg}H} \right\} \\ &= \sum_{n=1}^{N_G} \int_0^{2\pi} \int_0^{R_{\text{bs}}} \frac{c^2 M_x M_y G_T G_R \mathbf{V}_n^{\text{sg}}(r_n, \phi_n) f(r_n, \phi_n) r_n dr_n d\phi_n}{(4\pi f d_n(r_n, \phi_n))^2}, \end{aligned} \quad (10)$$

where N_G and \bar{K}_G are the numbers of terrestrial BSs and UTs per BS, respectively. We have $\mathbb{E} \{ |g_{n,k}^{\text{sg}}(t, f)|^2 \} = (\gamma_{n,k}^{\text{sg}})^2 = \frac{M_x M_y G_T G_R c^2}{(4\pi f d_{n,k})^2}$ and $\mathbf{V}_n^{\text{sg}}(r_n, \phi_n) = \mathbf{v}_n^{\text{sg}}(r_n, \phi_n) \mathbf{v}_n^{\text{sg}}(r_n, \phi_n)^H$. G_T and G_R are the per-antenna transmit gain and receive gain, respectively. $f(r_n, \phi_n)$ is the probability density function of user distribution. The propagation distance between the satellite and the UT at the n -th terrestrial BS, given the UT's polar coordinates ϕ_n and r_n representing the angular and radial positions, respectively, can be computed by

$$d_n(r_n, \phi_n) = \sqrt{h_{\text{sat}}^2 + R_n^2 + r_n^2 + 2R_n r_n \cos(\psi_n - \phi_n)}, \quad (11)$$

where h_{sat} denotes the satellite height, ψ_n the polar angle of the n -th terrestrial BS, and R_n the distance from the n -th terrestrial BS to the sub-satellite point. Then we compute the (i, j) -th element of $\mathbf{V}_n^{\text{sg}}(r_n, \phi_n)$ as

$$[\mathbf{V}_n^{\text{sg}}(r_n, \phi_n)]_{i,j} = \frac{e^{j\pi[(m_a - m_p)\vartheta_n^x + (n_b - n_q)\vartheta_n^y]}}{M_x M_y}. \quad (12)$$

The element indices are determined by the expressions $i = n_q M_x + m_p + 1$ and $j = n_b M_x + m_a + 1$, where the indices follow the ordering: $n_q = 0, \dots, M_y - 1$, $m_p = 0, \dots, M_x - 1$, $n_b = 0, \dots, M_y - 1$ and $m_a = 0, \dots, M_x - 1$. The channel space angles are computed as $\vartheta_n^x(r_n, \phi_n) =$

$\frac{R_n \cos \psi_n + r_n \cos \phi_n}{R_{\text{sat}}}$ and $\vartheta_n^y(r_n, \phi_n) = \frac{R_n \sin \psi_n + r_n \sin \phi_n}{R_{\text{sat}}}$ where R_{sat} is the satellite coverage radius. To simplify, we replace $\varpi_n(r_n, \phi_n) = (m_a - m_p)\vartheta_n^x + (n_b - n_q)\vartheta_n^y$. Thus, we obtain the integral form of the interference channel term $\mathbf{\Upsilon}_{\text{sg}}^{\text{int}}$, and its (i, j) -th element can be rewritten as

$$[\mathbf{\Upsilon}_{\text{sg}}^{\text{int}}]_{i,j} = \sum_{n=1}^{N_G} \int_0^{2\pi} \int_0^{R_{\text{bs}}} \frac{G_T G_R c^2 e^{j\pi \varpi_n(r_n, \phi_n)}}{(4\pi f d_n(r_n, \phi_n))^2} \times f(r_n, \phi_n) r_n dr_n d\phi_n. \quad (13)$$

This integral-form interference model, free of shared CSI from terrestrial UTs, leverages BS positions and terrestrial user distribution, thereby reducing the need for extensive pilot overhead, latency, and computational complexity.

In Sections III and IV, we use the integral-form interference channel term $\mathbf{\Upsilon}_{\text{sg}}^{\text{int}}$, which is free of shared CSI, along with sCSI, including $\mathbb{E}\{g_k^{\text{ss}}(t, f)\}$ and $\mathbb{E}\{\mathbf{H}_{\text{ss}}\mathbf{H}_{\text{ss}}^H\}$, to design robust TX beamforming under the interference threshold. In Section V, we further utilize the information of terrestrial BS positions to approximate the integral-form interference channel term $\mathbf{\Upsilon}_{\text{sg}}^{\text{int}}$, which avoids the complex integral calculations.

III. SUM RATE MAXIMIZATION BEAMFORMING UNDER INTERFERENCE THRESHOLD

A. Problem Formulation

In this subsection, we design beamforming to maximize the weighted sum rate while ensuring that the average satellite-to-terrestrial UT interference remains below the threshold I_{thr} , whose optimization problem can be formulated as follows

$$\begin{aligned} \max_{\mathbf{P}} \quad & \sum_{k=1}^{K_S} \mathbb{E}_{\mathbf{H}_{\text{ss}}} \left\{ a_k \log_2 \left(1 + \frac{\mathbf{p}_k^H \mathbf{h}_{\text{ss},k} \mathbf{h}_{\text{ss},k}^H \mathbf{p}_k}{\sum_{i \neq k} \mathbf{p}_i^H \mathbf{h}_{\text{ss},k} \mathbf{h}_{\text{ss},k}^H \mathbf{p}_i + \sigma_k^2} \right) \right\}, \\ \text{s.t.} \quad & \frac{1}{K_G} \text{Tr} \{ \mathbf{P}^H \mathbf{\Upsilon}_{\text{sg}}^{\text{int}} \mathbf{P} \} \leq I_{\text{thr}}, \\ & \text{Tr} \{ \mathbf{P} \mathbf{P}^H \} \leq P_T, \end{aligned} \quad (14)$$

where P_T denotes the antenna power budget and a_k represents the weight for the k -th satellite UT.

Proposition 1. Problem (14) is equivalent to problem (15), in the sense that the global optimal solution for the two problems is identical.

$$\begin{aligned} \max_{\mathbf{P}} \quad & \sum_{k=1}^{K_S} \mathbb{E}_{\mathbf{B}} \left\{ a_k \log_2 \left(1 + \frac{\mathbf{p}_k^H \mathbf{b}_k \mathbf{b}_k^H \mathbf{p}_k}{\sum_{i \neq k} \mathbf{p}_i^H \mathbf{b}_k \mathbf{b}_k^H \mathbf{p}_i + \sigma_k^2} \right) \right\}, \\ \text{s.t.} \quad & \frac{1}{K_G} \text{Tr} \{ \mathbf{P}^H \mathbf{\Upsilon}_{\text{sg}}^{\text{int}} \mathbf{P} \} \leq I_{\text{thr}}, \\ & \text{Tr} \{ \mathbf{P} \mathbf{P}^H \} \leq P_T, \end{aligned} \quad (15)$$

where we define $\mathbf{b}_k = g_k^{\text{ss}}(t, f) \mathbf{v}_k^{\text{ss}}$ and $\mathbf{B} = [\mathbf{b}_1, \dots, \mathbf{b}_{K_S}] \in \mathbb{C}^{M_S \times K_S}$ representing the satellite-to-satellite UT channel matrix which ignores the phase information.

Proof. See Appendix A.

Proposition 1 shows that we can obtain an optimal solution to problem (14) by solving problem (15). However, prob-

$$f(\boldsymbol{\xi}, \mathbf{P}) = \sum_{k=1}^{K_S} a_k \log_2 \left(1 + 2 \operatorname{Re} \{ \xi_k^* \bar{\mathbf{h}}_k^H \mathbf{p}_k \} - \xi_k^* \left(\sum_{i=1}^{K_S} \mathbf{p}_i^H \boldsymbol{\Upsilon}_{ss,k} \mathbf{p}_i - \mathbf{p}_k^H \bar{\mathbf{h}}_k \bar{\mathbf{h}}_k^H \mathbf{p}_k + \sigma_k^2 \right) \xi_k \right). \quad (18)$$

Algorithm 1 WSR-MCQT-Based TX Beamforming

1: **Input:** $\{\mathbf{v}_k^{ss}, \gamma_k^{ss}, \bar{\gamma}_k^{ss}, \sigma_k^2\}_{k=1}^{K_S}$, $\boldsymbol{\Upsilon}_{sg}^{\text{int}}$, I_{thr} , P_T , Iter_{max} , δ .
2: Initialize the beamforming matrix \mathbf{P} , $f^{(0)}$ and $n = 1$.
3: **while** $n < \text{Iter}_{\text{max}}$ **do**
4: Calculate auxiliary variable $\{\xi_k^*\}_{k=1}^{K_S}$ from (20).
5: Obtain \mathbf{P}^* by solving problem (21).
6: Calculate $f^{(n)}$ and $I_{\text{avg}}^{(n)}$.
7: **if** $|f^{(n)} - f^{(n-1)}| < \delta$ **and** $I_{\text{avg}}^{(n)} < I_{\text{thr}}$
8: **break**
9: **end if**
10: $n = n + 1$.
11: **end while**
12: **Output:** $\boldsymbol{\xi}^*$ and \mathbf{P}^* .

lem (15) still constitutes a non-convex optimization problem, which poses significant challenges in obtaining the globally optimal solution.

B. Alternating Optimization Algorithm based on MCQT

According to *Jensen's inequality*, the ergodic sum rate, i.e. the objective function in (15), is lower bounded by [52]

$$\begin{aligned} & \sum_{k=1}^{K_S} \mathbb{E}_{\mathbf{B}} \left\{ a_k \log_2 \left(1 + \frac{\mathbf{p}_k^H \mathbf{b}_k \mathbf{b}_k^H \mathbf{p}_k}{\sum_{i \neq k} \mathbf{p}_i^H \mathbf{b}_k \mathbf{b}_k^H \mathbf{p}_i + \sigma_k^2} \right) \right\} \\ & \geq \sum_{k=1}^{K_S} a_k \log_2 \left(1 + \frac{\mathbf{p}_k^H \bar{\mathbf{h}}_k \bar{\mathbf{h}}_k^H \mathbf{p}_k}{\sum_{i=1}^{K_S} \mathbf{p}_i^H \boldsymbol{\Upsilon}_{ss,k} \mathbf{p}_i - \mathbf{p}_k^H \bar{\mathbf{h}}_k \bar{\mathbf{h}}_k^H \mathbf{p}_k + \sigma_k^2} \right), \end{aligned} \quad (16)$$

where we define $\bar{\mathbf{h}}_k = \mathbb{E} \{ \mathbf{b}_k \} = \bar{\gamma}_k^{ss} \mathbf{v}_k^{ss}$ and $\boldsymbol{\Upsilon}_{ss,k} = \mathbb{E} \{ \mathbf{b}_k \mathbf{b}_k^H \} = (\gamma_k^{ss})^2 \mathbf{v}_k^{ss} \mathbf{v}_k^{ssH}$. As such, we reformulate the direct maximization of the ergodic sum rate as the maximization of its lower bound. Since this problem is a standard concave-convex multiple-ratio fractional programming problem, we apply the multidimensional complex quadratic transformation (MCQT) to tackle it. This transformation decouples the numerator and denominator of each SINR through MCQT decoupling [53]. Consequently, the original WSR problem (14) is transformed into

$$\begin{aligned} & \max_{\boldsymbol{\xi}, \mathbf{P}} f(\boldsymbol{\xi}, \mathbf{P}), \\ & \text{s.t.} \quad \frac{1}{K_G} \operatorname{Tr} \{ \mathbf{P}^H \boldsymbol{\Upsilon}_{sg}^{\text{int}} \mathbf{P} \} \leq I_{\text{thr}}, \\ & \quad \operatorname{Tr} \{ \mathbf{P} \mathbf{P}^H \} \leq P_T, \end{aligned} \quad (17)$$

where $\boldsymbol{\xi} \in \mathbb{C}^{K_S \times 1}$ denotes the auxiliary variable, and the objective function given by (18) is convex with respect to $\boldsymbol{\xi}$ and \mathbf{P} , respectively.

On the basis of this transformation, we propose an alternating optimization algorithm to address this problem. Specifically, when matrix \mathbf{P} is fixed, the problem becomes an unconstrained convex optimization as $\max_{\boldsymbol{\xi}} f(\boldsymbol{\xi}, \mathbf{P})$. Here,

the optimal solution ξ_k^* can be obtained by setting the $\nabla_{\boldsymbol{\xi}} f(\boldsymbol{\xi})$ to zero, as shown below

$$\begin{aligned} \xi_k^* &= \frac{\bar{\mathbf{h}}_k^H \mathbf{p}_k}{\sum_{i=1}^{K_S} \mathbf{p}_i^H \boldsymbol{\Upsilon}_{ss,k} \mathbf{p}_i - \mathbf{p}_k^H \bar{\mathbf{h}}_k \bar{\mathbf{h}}_k^H \mathbf{p}_k + \sigma_k^2} \\ &= \frac{(\bar{\gamma}_k^{ss})^* (\mathbf{v}_k^{ss})^H \mathbf{p}_k}{\sum_{i=1}^{K_S} (\gamma_k^{ss})^2 \mathbf{p}_i^H \mathbf{v}_k^{ss} (\mathbf{v}_k^{ss})^H \mathbf{p}_i - |\bar{\gamma}_k^{ss}|^2 \mathbf{p}_k^H \mathbf{v}_k^{ss} (\mathbf{v}_k^{ss})^H \mathbf{p}_k + \sigma_k^2}. \end{aligned} \quad (19)$$

With the auxiliary variable $\boldsymbol{\xi}^*$ fixed, the original optimization problem in (17) can be transformed into

$$\begin{aligned} & \max_{\mathbf{P}} f(\mathbf{P}), \\ & \text{s.t.} \quad \frac{1}{K_G} \operatorname{Tr} \{ \mathbf{P}^H \boldsymbol{\Upsilon}_{sg}^{\text{int}} \mathbf{P} \} \leq I_{\text{thr}}, \\ & \quad \operatorname{Tr} \{ \mathbf{P} \mathbf{P}^H \} \leq P_T. \end{aligned} \quad (21)$$

The above problem is a convex problem and can be solved with generic convex optimization algorithms, e.g., the interior point algorithm [54]. The optimization of $\boldsymbol{\xi}$ and \mathbf{P} alternates until convergence, and this process is summarized in **Algorithm 1**.

The computational complexity of **Algorithm 1** is dominated by Step 5 and Step 6. Specifically, Step 5 solving for \mathbf{P}^* using the interior-point method performs with a complexity order of $\mathcal{O}(T_A (M_S^3 K_S^3))$, assuming a maximum of T_A inner loop iterations; Step 6 performs the matrix multiplication for the calculation of the objective function and the computation of average interference, involving both integral calculation and matrix multiplication, has a complexity order of $\mathcal{O}(M_S K_S^2 + M_S^2 N_G N_r N_\phi)$. Herein, N_r and N_ϕ denote the numbers of discrete samples for the integral over the terrestrial BS radius r and the polar angle ϕ , respectively. Thus, the total complexity order of **Algorithm 1** is $\mathcal{O}(T_A (M_S^3 K_S^3) + M_S^2 N_G N_r N_\phi)$ per iteration.

C. WMMSE Algorithm under Interference Threshold

Although the scheme in Section III-B achieves outstanding performance, the subproblem in (21) still incurs high computational complexity due to the large dimension of \mathbf{P} . Therefore, in this subsection, we propose an iterative algorithm derived from the equivalence between the WSR and WMMSE problems, termed WSR-WMMSE equivalence (WWE), which leverages the KKT conditions of the WMMSE problem to facilitate a solving process with lower computational complexity. With the definitions $\mathbf{u} \in \mathbb{C}^{K_S \times 1}$ and $\mathbf{w} \in \mathbb{C}^{K_S \times 1}$, the following WMMSE problem

$$\begin{aligned} & \min_{\mathbf{u}, \mathbf{w}, \mathbf{P}} \sum_{k=1}^{K_S} (w_k e_k - \log w_k), \\ & \text{s.t.} \quad \frac{1}{K_G} \operatorname{Tr} \{ \mathbf{P}^H \boldsymbol{\Upsilon}_{sg}^{\text{int}} \mathbf{P} \} \leq I_{\text{thr}}, \\ & \quad \operatorname{Tr} \{ \mathbf{P} \mathbf{P}^H \} \leq P_T, \end{aligned} \quad (22)$$

is equivalent to the WSR problem in (14) with the lower bound objective in (16), in the sense that the global optimal solution \mathbf{P} for the two problems are identical [55], [56]. The MSE e_k can be expressed as

$$\begin{aligned} e_k &= \mathbb{E}_{\mathbf{b}_k, \mathbf{x}_s, n_k} \left\{ |u_k (\mathbf{b}_k^H \mathbf{P} \mathbf{x}_s + n_k) - x_k|^2 \right\} \\ &= |u_k|^2 \left(\sum_{i=1}^{K_S} \mathbf{p}_i^H \mathbf{\Upsilon}_{ss,k} \mathbf{p}_i + \sigma_k^2 \right) - u_k^* \mathbf{p}_k^H \bar{\mathbf{h}}_k - u_k \bar{\mathbf{h}}_k^H \mathbf{p}_k + 1. \end{aligned} \quad (23)$$

Therefore, with \mathbf{P} and \mathbf{w} fixed, the optimal value of u_k^* can be determined by setting the derivative of $e_k(u_k)$ with respect to u_k^* equal to zero

$$\begin{aligned} u_k^* &= \frac{\mathbf{p}_k^H \bar{\mathbf{h}}_k}{\sum_{i=1}^{K_S} \mathbf{p}_i^H \mathbf{\Upsilon}_{ss,k} \mathbf{p}_i + \sigma_k^2} \\ &= \frac{\bar{\gamma}_k^{ss} \mathbf{p}_k^H \mathbf{v}_k^{ss}}{\sum_{i=1}^{K_S} (\gamma_k^{ss})^2 \mathbf{p}_i^H \mathbf{v}_k^{ss} \mathbf{v}_k^{ssH} \mathbf{p}_i + \sigma_k^2}. \end{aligned} \quad (24)$$

At this point, the value of e_k can be computed as

$$\begin{aligned} e_k &= 1 - \frac{\mathbf{p}_k^H \bar{\mathbf{h}}_k \bar{\mathbf{h}}_k^H \mathbf{p}_k}{\sum_{i=1}^{K_S} \mathbf{p}_i^H \mathbf{\Upsilon}_{ss,k} \mathbf{p}_i + \sigma_k^2} \\ &= 1 - \frac{|\bar{\gamma}_k^{ss}|^2 \mathbf{p}_k^H \mathbf{v}_k^{ss} \mathbf{v}_k^{ssH} \mathbf{p}_k}{\sum_{i=1}^{K_S} (\gamma_k^{ss})^2 \mathbf{p}_i^H \mathbf{v}_k^{ss} \mathbf{v}_k^{ssH} \mathbf{p}_i + \sigma_k^2}. \end{aligned} \quad (25)$$

The equivalence between the WSR and WMMSE problems can be established when the KKT conditions of both problems are simultaneously satisfied [30]. By equating the gradients of their respective Lagrangian functions, the optimal MSE-weights $\{w_k\}_{k=1}^{K_S}$ can be derived for given \mathbf{P} and \mathbf{u}^* as [56]

$$w_k^* = a_k e_k^{-1}. \quad (26)$$

Then we fix vectors \mathbf{w}^* and \mathbf{u}^* , the optimization problem is reduced to

$$\begin{aligned} \min_{\mathbf{P}} \quad & \epsilon(\mathbf{P}) = \sum_{k=1}^{K_S} w_k e_k(\mathbf{P}), \\ \text{s.t.} \quad & \frac{1}{K_G} \text{Tr} \{ \mathbf{P}^H \mathbf{\Upsilon}_{sg}^{\text{int}} \mathbf{P} \} \leq I_{\text{thr}}, \\ & \text{Tr} \{ \mathbf{P} \mathbf{P}^H \} \leq P_T, \end{aligned} \quad (27)$$

whose Lagrange function can be derived as

$$\begin{aligned} \mathcal{L}(\mathbf{P}) &= \sum_{k=1}^{K_S} w_k e_k(\mathbf{P}) + \lambda (\text{Tr} \{ \mathbf{P} \mathbf{P}^H \} - P_T) \\ &\quad + \mu \left(\frac{1}{K_G} \text{Tr} \{ \mathbf{P}^H \mathbf{\Upsilon}_{sg}^{\text{int}} \mathbf{P} \} - I_{\text{thr}} \right), \end{aligned} \quad (28)$$

where λ and μ are the Lagrange multipliers. By setting $\nabla_{\mathbf{P}^*} \mathcal{L} = \mathbf{0}$, we formulate the closed-form iterative expression for \mathbf{P}^* as

$$\mathbf{P}^*(\lambda, \mu) = \left(\hat{\mathbf{\Upsilon}}_{ss} + \lambda \mathbf{I} + \frac{\mu}{K_G} \mathbf{\Upsilon}_{sg}^{\text{int}} \right)^{-1} \mathbf{W} \mathbf{U}^H \bar{\mathbf{H}}_{ss}, \quad (29)$$

where we denote $\hat{\mathbf{\Upsilon}}_{ss} = \sum_{k=1}^{K_S} u_k^* w_k u_k \mathbb{E} \{ \mathbf{b}_k \mathbf{b}_k^H \} = \sum_{k=1}^{K_S} u_k^* w_k u_k (\gamma_k^{ss})^2 \mathbf{v}_k^{ss} \mathbf{v}_k^{ssH}$. Moreover, we define matrices $\mathbf{W}^* = \text{diag} \{ [w_1, \dots, w_{K_S}] \}$, $\mathbf{U}^* = \text{diag} \{ [u_1, \dots, u_{K_S}] \}$ and $\bar{\mathbf{H}}_{ss} = \mathbb{E} \{ \mathbf{B} \}$. By substituting this expression into

Algorithm 2 WVE-Based TX Beamforming

```

1: Input:  $\{\mathbf{v}_k^{ss}, \gamma_k^{ss}, \bar{\gamma}_k^{ss}, \sigma_k^2\}_{k=1}^{K_S}$ ,  $\mathbf{\Upsilon}_{sg}^{\text{int}}$ ,  $I_{\text{thr}}$ ,  $P_T$ ,  $\text{Iter}_{\text{max}}$ ,  $\delta$ .
2: Initialize the beamforming matrix  $\mathbf{P}$ ,  $\epsilon^{(0)}$  and  $n = 1$ .
3: while  $n < \text{Iter}_{\text{max}}$  do
4:   Calculate  $\{u_k^*\}_{k=1}^{K_S}$  and  $\{w_k^*\}_{k=1}^{K_S}$  from (24) and (26).
5:   Solve  $\lambda^{(n)}$  and  $\mu^{(n)}$  from problem (30).
6:   Calculate  $\mathbf{P}^*$  from (29).
7:   Calculate  $\epsilon^{(n)}$  and  $I_{\text{avg}}^{(n)}$ .
8:   if  $|\epsilon^{(n)} - \epsilon^{(n-1)}| < \delta$  and  $I_{\text{avg}}^{(n)} < I_{\text{thr}}$ 
9:     break
10:  end if
11:   $n = n + 1$ .
12: end while
13: Output:  $\mathbf{P}^*$ .

```

problem (27), it can be reduced as the following optimization problem in terms of λ and μ

$$\begin{aligned} \min_{\lambda, \mu} \quad & \epsilon(\lambda, \mu) = \sum_{k=1}^{K_S} w_k e_k(\lambda, \mu), \\ \text{s.t.} \quad & \frac{1}{K_G} \text{Tr} \{ \mathbf{P}^H(\lambda, \mu) \mathbf{\Upsilon}_{sg}^{\text{int}} \mathbf{P}(\lambda, \mu) \} \leq I_{\text{thr}}, \\ & \text{Tr} \{ \mathbf{P}(\lambda, \mu) \mathbf{P}^H(\lambda, \mu) \} \leq P_T. \end{aligned} \quad (30)$$

Although the above problem is non-convex, its low-dimensional optimization variable allows us to solve it efficiently by conventional iterative algorithms. After this, by bringing λ^* and μ^* back to formula (29), we can get the result of \mathbf{P}^* without loss of performance. It is worth noting that, within the alternating optimization framework, rather than searching for the optimal solution of \mathbf{P} in (27), we can focus on finding feasible solutions that lead to a decreasing objective function. This approach provides further reductions in the computational complexity, while also ensuring gradual improvement of the original optimization objective. In conclusion, we optimize the Lagrange multipliers λ and μ in each iteration, and update \mathbf{u}^* , \mathbf{w}^* and \mathbf{P}^* alternately until convergence, summarized in **Algorithm 2**.

The computational complexity of **Algorithm 2** primarily arises from Steps 5 and 6. Specifically, Step 5 solving for λ and μ using the interior point method involves a complexity order of $\mathcal{O}(T_B)$ where T_B represents the maximum number of inner iterations; Step 6, which involves calculating \mathbf{P}^* , has a complexity order of $\mathcal{O}(M_S^2 K_S + M_S^2 N_G N_r N_\phi + M_S^3)$. Consequently, the overall complexity order of **Algorithm 2** per iteration is $\mathcal{O}(T_B + M_S^2 K_S + M_S^2 N_G N_r N_\phi + M_S^3)$, which represents a significant reduction compared to **Algorithm 1**.

IV. CLOSED-FORM TX BEAMFORMING BASED ON MMSE FOR INTERFERENCE AVOIDANCE

As another linear beamforming design criterion, MMSE is widely adopted due to its significant enhancement of demodulation performance and the availability of closed-form optimal solutions in many cases. In this section, we revisit the MMSE beamforming design under the constraint of inter-system interference and based on the available sCSI.

A. Problem Formulation

The TX beamforming optimization problem with the MMSE criterion under the interference threshold is formulated as follows

$$\begin{aligned} \min_{\mathbf{P}, \beta} \quad & \mathbb{E}_{\mathbf{H}_{ss}, \mathbf{x}_s, \mathbf{n}_s} \left\{ \left\| \frac{\mathbf{\Psi}_s (\mathbf{H}_{ss}^H \mathbf{P} \mathbf{x}_s + \mathbf{n}_s)}{\beta} - \mathbf{x}_s \right\|_2^2 \right\}, \\ \text{s.t.} \quad & \frac{1}{K_G} \text{Tr} \{ \mathbf{P}^H \mathbf{\Upsilon}_{sg}^{\text{int}} \mathbf{P} \} \leq I_{\text{thr}}, \\ & \text{Tr} \{ \mathbf{P} \mathbf{P}^H \} \leq P_T. \end{aligned} \quad (31)$$

Herein, $\mathbf{\Psi}_s = \text{diag} \{ [e^{j\psi_1}, \dots, e^{j\psi_{K_s}}] \}$ represents the phase compensation for delay and Doppler shifts at the receiver with $\psi_k = 2\pi (tv_k^{\text{sat}} - f\tau_k^{\text{min}})$. Compared to the difficulty of phase compensation at the transmitter, the receiver can accurately estimate phase errors based on downlink pilot signals to assist with compensation [57], [58]. To simplify the problem, we employ the penalty function method to mitigate interference [59]. Specifically, we introduce a penalty term $\bar{\varsigma} \text{Tr} \{ \mathbf{P}^H \mathbf{\Upsilon}_{sg}^{\text{int}} \mathbf{P} \}$ into the objective function, transforming the problem into a convex optimization problem subject to power budget. Here, $\bar{\varsigma}$ represents the penalty factor, and for the sake of derivation, we set $\bar{\varsigma} = \frac{\varsigma}{\beta^2}$, allowing us to rewrite the optimization problem as follows

$$\begin{aligned} \min_{\mathbf{P}, \beta} \quad & \mathbb{E}_{\mathbf{H}_{ss}, \mathbf{x}_s, \mathbf{n}_s} \left\{ \left\| \frac{\mathbf{\Psi}_s (\mathbf{H}_{ss}^H \mathbf{P} \mathbf{x}_s + \mathbf{n}_s)}{\beta} - \mathbf{x}_s \right\|_2^2 \right\} + \bar{\varsigma} \text{Tr} \{ \mathbf{P}^H \mathbf{\Upsilon}_{sg}^{\text{int}} \mathbf{P} \}, \\ \text{s.t.} \quad & \text{Tr} \{ \mathbf{P} \mathbf{P}^H \} \leq P_T. \end{aligned} \quad (32)$$

Proposition 2. *The following solution achieves the optimum of problem (32), where*

$$\mathbf{P}^* = \beta^* \left(\mathbf{\Upsilon}_{ss} + \varsigma \mathbf{\Upsilon}_{sg}^{\text{int}} + \frac{K_S \sigma_s^2}{P_T} \mathbf{I} \right)^{-1} \bar{\mathbf{H}}_{ss}, \quad (33)$$

$$\beta^* = \sqrt{\frac{P_T}{\left\| \left(\mathbf{\Upsilon}_{ss} + \varsigma \mathbf{\Upsilon}_{sg}^{\text{int}} + \frac{K_S \sigma_s^2}{P_T} \mathbf{I} \right)^{-1} \bar{\mathbf{H}}_{ss} \right\|_F^2}}, \quad (34)$$

where $\mathbf{\Upsilon}_{ss} \triangleq \mathbb{E} \{ \mathbf{H}_{ss} \mathbf{H}_{ss}^H \} = \sum_{k=1}^{K_S} (\gamma_k^{\text{ss}})^2 \mathbf{v}_k^{\text{ss}} \mathbf{v}_k^{\text{ss}H}$ and it is assumed that $\sigma_k^2 = \sigma_s^2$ for all UTs.

Proof. See Appendix B.

Remark 1. When both \mathbf{W} and \mathbf{U} are identity matrices, and by forcing $\lambda = \frac{K_S \sigma_s^2}{P_T}$ and $\mu = \varsigma K_G$, the beamforming matrix in formula (29) can degenerate into the closed-form MMSE solution in formula (33).

B. Closed-Form Beamforming under Interference Threshold

The selection of ς is crucial, as it effectively represents the trade-off between MMSE performance and interference management capability. Specifically, the relationship is summarized in **Proposition 3**.

Proposition 3. *For the closed-form solution of \mathbf{P} in (33), the derivative of the total interference I_{sg} with respect to ς is*

Algorithm 3 Closed-Form TX Beamforming

- 1: **Input:** $\{ \mathbf{v}_k^{\text{ss}}, \gamma_k^{\text{ss}}, \bar{\gamma}_k^{\text{ss}} \}_{k=1}^{K_S}, \mathbf{\Upsilon}_{sg}^{\text{int}}, I_{\text{thr}}, P_T, \sigma_s^2$.
- 2: Find ς for given I_{thr} and SNR via a bisection method.
- 3: $\beta^* = \sqrt{P_T / \left\| \left(\mathbf{\Upsilon}_{ss} + \varsigma \mathbf{\Upsilon}_{sg}^{\text{int}} + \frac{K_S \sigma_s^2}{P_T} \mathbf{I} \right)^{-1} \bar{\mathbf{H}}_{ss} \right\|_F^2}$.
- 4: $\mathbf{P}^* = \beta^* \left(\mathbf{\Upsilon}_{ss} + \varsigma \mathbf{\Upsilon}_{sg}^{\text{int}} + \frac{K_S \sigma_s^2}{P_T} \mathbf{I} \right)^{-1} \bar{\mathbf{H}}_{ss}$.
- 5: **Output:** β^* and \mathbf{P}^* .

non-positive.

$$\nabla_{\varsigma} I_{sg}(\varsigma) = \frac{\partial I_{sg}(\varsigma)}{\partial \varsigma} = \frac{\partial \text{Tr} \{ \mathbf{P}^H(\varsigma) \mathbf{\Upsilon}_{sg}^{\text{int}} \mathbf{P}(\varsigma) \}}{\partial \varsigma} \leq 0. \quad (35)$$

Proof. See Appendix C.

Given that a higher value of ς results in a lower interference power I_{sg} , the value of ς corresponding to a fixed average interference threshold I_{thr} and a specific signal-to-noise ratio (SNR) can be determined through a bisection method. The detailed algorithm is described in **Algorithm 3**.

Although the bisection method requires iterative calculations of the beamforming matrix when performing TX beamforming over continuous time slots or beamforming periods, we can significantly reduce the frequency of executing the bisection method by predicting the variation of ς . This approach enables the beamforming scheme to be approximated as a closed-form computation. Upon analyzing the solution of \mathbf{P}^* , the overall complexity order is $\mathcal{O}(M_S^2 N_G N_r N_\phi + M_S^3)$. Compared to the iterative solutions for the beamforming matrix discussed in the previous section, this closed-form beamforming solution significantly reduces the computational complexity.

V. POSITION-AIDED INTERFERENCE APPROXIMATION IN TX BEAMFORMING DESIGN

In the proposed schemes, the TX beamforming relies on the integral term $\mathbf{\Upsilon}_{sg}^{\text{int}}$. However, this integral term is computationally intensive and requires a real-time distribution of terrestrial users, which poses practical challenges. To address these issues, we leverage the information of terrestrial BS positions to approximate $\mathbf{\Upsilon}_{sg}^{\text{int}}$, thereby eliminating reliance on the integral of terrestrial user distribution and significantly reducing the overall computational complexity of the beamforming schemes. We call this approximation process the terrestrial BS position-aided (PA) method. Specifically, positions of terrestrial BSs are assumed to be prior knowledge due to their fixed and planned deployment, allowing the satellite to compute the angular parameters (e.g., azimuth and elevation) via geometric relationships. Based on this, the satellite-to-BS channel is estimated with the Rician factor inferred from angular information [45].

As depicted in Fig. 2, the coverage area of the terrestrial BS cell is significantly smaller than the size of satellite beams [22]. Therefore, we approximate the satellite-to-terrestrial UT interference channel as the corresponding satellite-to-terrestrial BS channel. We define $\tilde{\mathbf{H}}_{sg}$ to represent the channel from the satellite to the terrestrial BSs and the approximation of $\mathbf{\Upsilon}_{sg}^{\text{int}}$ can be expressed as $\tilde{\mathbf{\Upsilon}}_{sg} = \bar{K}_G \mathbb{E} \{ \tilde{\mathbf{H}}_{sg} \tilde{\mathbf{H}}_{sg}^H \}$ where \bar{K}_G is

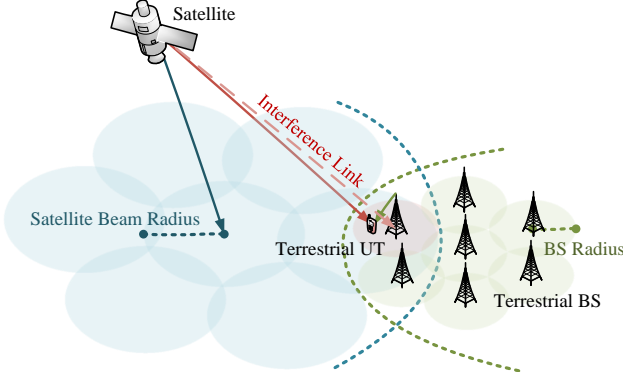


Fig. 2. Approximation of terrestrial UTs with terrestrial BS position.

the number of UTs per terrestrial BS. The original constraint of average interference power can be approximated as

$$\begin{aligned} & \frac{1}{K_G} \text{Tr} \left\{ \mathbf{P}^H \bar{K}_G \mathbb{E} \left\{ \tilde{\mathbf{H}}_{\text{sg}} \tilde{\mathbf{H}}_{\text{sg}}^H \right\} \mathbf{P} \right\} \\ &= \frac{1}{K_G} \text{Tr} \left\{ \mathbf{P}^H \tilde{\mathbf{\Upsilon}}_{\text{sg}} \mathbf{P} \right\} \leq I_{\text{thr}}. \end{aligned} \quad (36)$$

The other steps in Section III remain unchanged, except for the formula in (29) based on the equivalence between the WSR and WMMSE problems, which needs to be modified as

$$\mathbf{P}_{\text{WWEIA-PA}} = \left(\hat{\mathbf{\Upsilon}}_{\text{ss}} + \lambda \mathbf{I} + \frac{\mu}{K_G} \tilde{\mathbf{\Upsilon}}_{\text{sg}} \right)^{-1} \mathbf{W} \mathbf{U}^H \bar{\mathbf{H}}_{\text{ss}}. \quad (37)$$

Similarly, in Section IV, we also need to modify the original closed-form solution with the MMSE criterion in (33) as

$$\mathbf{P}_{\text{MMSEIA-PA}} = \beta \left(\mathbf{\Upsilon}_{\text{ss}} + \varsigma \tilde{\mathbf{\Upsilon}}_{\text{sg}} + \frac{K_S \sigma_s^2}{P_T} \mathbf{I} \right)^{-1} \bar{\mathbf{H}}_{\text{ss}}. \quad (38)$$

Considering that the approximation may introduce an error that could degrade performance, we further analyze the factors influencing the approximation error.

Proposition 4. Assuming that the terrestrial users of the single terrestrial BS located at the sub-satellite point follow a uniform distribution within the terrestrial BS radius R_{bs} , and the user density is ρ_{tut} . The (i, j) -th element of the squared error matrix $\mathcal{E}_{\text{sg}} \in \mathbb{R}^{M_S \times M_S}$ between the integral-form expression $\mathbf{\Upsilon}_{\text{sg}}^{\text{int}}$ and its approximation $\tilde{\mathbf{\Upsilon}}_{\text{sg}}$ can be computed as

$$[\mathcal{E}_{\text{sg}}]_{i,j} = \eta^2 \left| \frac{\pi R_{\text{bs}}^2}{h_{\text{sat}}^2} - \int_0^{R_{\text{bs}}} \frac{2\pi r J_0\left(\frac{\pi r \omega}{R_{\text{sat}}}\right) dr}{h_{\text{sat}}^2 + r^2} \right|^2, \quad (39)$$

where we define $\omega = \sqrt{(m_a - m_p)^2 + (n_b - n_q)^2}$ and $\eta = \frac{G_T G_R c^2 \rho_{\text{tut}}}{(4\pi f)^2}$. The gradients satisfy the following inequalities

$$\nabla_{R_{\text{bs}}} [\mathcal{E}_{\text{sg}}]_{i,j} \geq 0, \quad \nabla_{\rho_{\text{tut}}} [\mathcal{E}_{\text{sg}}]_{i,j} \geq 0, \quad \nabla_f [\mathcal{E}_{\text{sg}}]_{i,j} \leq 0. \quad (40)$$

Proof. According to equation (13), we can derive the error between the integral-form $\mathbf{\Upsilon}_{\text{sg}}^{\text{int}}$ and its approximation $\tilde{\mathbf{\Upsilon}}_{\text{sg}}$ as in (41).

Using the first kind of Bessel function $\int_0^{2\pi} e^{ja \sin \phi} d\phi = 2\pi J_0(a)$, the integral can be simplified as $[\mathcal{E}_{\text{sg}}]_{i,j} =$

$\eta^2 \left| \frac{\pi R_{\text{bs}}^2}{h_{\text{sat}}^2} - \int_0^{R_{\text{bs}}} \frac{2\pi r J_0\left(\frac{\pi r \omega}{R_{\text{sat}}}\right) dr}{h_{\text{sat}}^2 + r^2} \right|^2$. The gradient of $[\mathcal{E}_{\text{sg}}]_{i,j}$ with respect to R_{bs} is given

$$\begin{aligned} \nabla_{R_{\text{bs}}} [\mathcal{E}_{\text{sg}}]_{i,j} &= 2\eta^2 \left(\frac{2\pi R_{\text{bs}}}{h_{\text{sat}}^2} - \frac{2\pi R_{\text{bs}} J_0\left(\frac{\pi R_{\text{bs}} \omega}{R_{\text{sat}}}\right)}{h_{\text{sat}}^2 + R_{\text{bs}}^2} \right) \\ &\quad \times \left(\frac{\pi R_{\text{bs}}^2}{h_{\text{sat}}^2} - \int_0^{R_{\text{bs}}} \frac{2\pi r J_0\left(\frac{\pi r \omega}{R_{\text{sat}}}\right) dr}{h_{\text{sat}}^2 + r^2} \right), \end{aligned} \quad (42)$$

where we can deduce that

$$\frac{2\pi R_{\text{bs}} J_0\left(\frac{\pi R_{\text{bs}} \omega}{R_{\text{sat}}}\right)}{h_{\text{sat}}^2 + R_{\text{bs}}^2} \leq \frac{2\pi R_{\text{bs}}}{h_{\text{sat}}^2}, \quad \int_0^{R_{\text{bs}}} \frac{2\pi r J_0\left(\frac{\pi r \omega}{R_{\text{sat}}}\right) dr}{h_{\text{sat}}^2 + r^2} \leq \frac{\pi R_{\text{bs}}^2}{h_{\text{sat}}^2}. \quad (43)$$

Given that $\eta = \frac{G_T G_R c^2 \rho_{\text{tut}}}{(4\pi f)^2}$, we can derive the gradients inequalities: $\nabla_{R_{\text{bs}}} [\mathcal{E}_{\text{sg}}]_{i,j} \geq 0$, $\nabla_{\rho_{\text{tut}}} [\mathcal{E}_{\text{sg}}]_{i,j} \geq 0$, and $\nabla_f [\mathcal{E}_{\text{sg}}]_{i,j} \leq 0$.

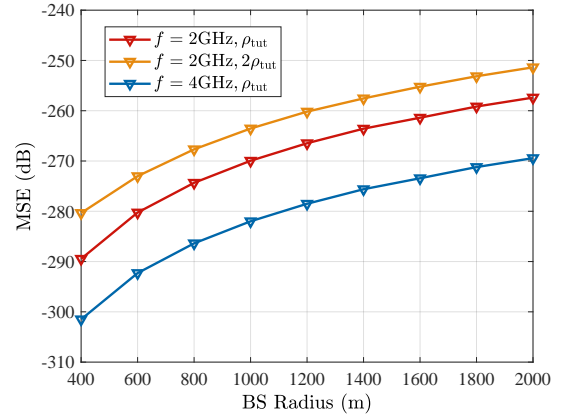


Fig. 3. The MSE between $\mathbf{\Upsilon}_{\text{sg}}^{\text{int}}$ and $\tilde{\mathbf{\Upsilon}}_{\text{sg}}$ vs R_{bs} , $\rho_{\text{tut}} = 0.0001/\text{m}^2$.

In addition, the simulation results presented in Fig. 3 validate the monotonic relationship between the terrestrial BS radius R_{bs} and the approximation error under varying carrier frequencies f and user densities ρ_{tut} . Specifically, we simulated the MSE of the approximate term for the single terrestrial BS located at the sub-satellite point. The results demonstrate that the MSE increases with the growth of the terrestrial BS radius R_{bs} and user density ρ_{tut} , while it decreases as the carrier frequency f increases.

Remark 2. This approximation refers to that when the position of the terrestrial UTs and the corresponding terrestrial BS exactly coincide, we have $\lim_{R_{\text{bs}} \rightarrow 0} [\mathcal{E}_{\text{sg}}]_{i,j} = 0$ and the approximate term $\tilde{\mathbf{\Upsilon}}_{\text{sg}}$ is identical to $\mathbf{\Upsilon}_{\text{sg}}^{\text{int}}$.

Remark 3. The computational complexity associated with the term $\mathbf{\Upsilon}_{\text{sg}}^{\text{int}}$ is significantly reduced when approximated by $\tilde{\mathbf{\Upsilon}}_{\text{sg}}$, with the complexity order decreasing from $\mathcal{O}(M_S^2 N_G N_r N_\phi)$ to $\mathcal{O}(M_S^2 N_G)$.

VI. NUMERICAL RESULTS

In this section, we employ the Monte Carlo method to evaluate the proposed schemes. We consider a sub-6GHz LEO satellite communication system, where the antenna elements are spaced at half-wavelength intervals along both the x and

$$[\mathcal{E}_{\text{sg}}]_{i,j} = \left| \left[\tilde{\mathbf{Y}}_{\text{sg}} \right]_{i,j} - \left[\mathbf{Y}_{\text{sg}}^{\text{int}} \right]_{i,j} \right|^2 = \eta^2 \left| \frac{\pi R_{\text{bs}}^2}{h_{\text{sat}}^2} - \int_0^{2\pi} \int_0^{R_{\text{bs}}} \frac{e^{\frac{j\pi}{R_{\text{sat}}} [(m_a - m_p)r \cos \phi + (n_b - n_q)r \sin \phi]} r dr d\phi}{h_{\text{sat}}^2 + r^2} \right|^2. \quad (41)$$

TABLE I
SATELLITE SYSTEM PARAMETERS [34], [45], [55]

Parameter	Value
Orbit Altitude h_{sat}	600 km
Satellite Coverage Radius R_{sat}	630 km
Carrier Frequency f	2 GHz
Number of Antennas M_S	8×8
Rician Factor κ_s	10 dB
Satellite Transmit Power P_T	25 dBW
Per-Antenna Gain G_T, G_R	6 dBi, 0 dBi
Noise Figure F	9 dB
Noise Temperature T	290 K

y axes [20]. During the simulation process, we focus on the LoS terrestrial UTs, which typically suffer stronger satellite interference and set the channel Rician factor to be $\kappa_k = \kappa_s$ for all UTs. The terrestrial BS has a coverage radius of 500 meters. We calculate $\text{SNR} = P_T - 10 \log K_S + G_T + 10 \log M_S - \text{PL} + G_R - 10 \log(k_{\text{bol}}[T + (F - 1)T_0]B)$ where k_{bol} , T_0 and B are the Boltzmann constant, standard temperature, and system bandwidth. The noise power σ_s^2 varies with the SNR. The remaining satellite system configurations are shown in Tab. I.

A. Performance Comparison of Beamforming Schemes

In this subsection, we validate the effectiveness of our TX beamforming algorithms and compare the following schemes:

- ‘**MRT**’/‘**ZF**’/‘**MMSE**’/‘**WMMSE**’ (Baseline): Four conventional linear TX beamforming [28]–[30].
- ‘**WQTIA**’: Robust TX beamforming based on MCQT for inter-system interference avoidance (IA) in Algorithm 1.
- ‘**WWEIA**’: Robust TX beamforming based on WWE for inter-system IA in Algorithm 2.
- ‘**MMSEIA**’: Closed-form robust TX beamforming based on MMSE for inter-system IA in Algorithm 3.

In Fig. 4, we present the beam patterns generated by different TX beamforming schemes. A comparison of these schemes reveals that the interference power at the positions of terrestrial UTs (indicated by green circles) is lower with the ‘**MMSEIA**’ scheme than with the ‘**MMSE**’ scheme, demonstrating the intuitive effect of interference mitigation.

Fig. 5 and Fig. 6 illustrate the comparison of the average interference power performance and sum rate of the satellite for a UPA configuration with $M_S = 8 \times 8$, satellite UT number $K_S = 12$, terrestrial BS number $N_G = 7$, terrestrial UT number per BS $\bar{K}_G = 10$, and an average interference threshold of $I_{\text{thr}} = -150$ dBW. In Fig. 5, the three TX beamforming schemes ‘**MMSEIA**’, ‘**WWEIA**’, and ‘**WQTIA**’ successfully achieve the interference threshold of -150 dBW at $\text{SNR} = 10$ dB. This performance illustrates their effectiveness in interference management. In Fig. 6, the ‘**MMSEIA**’ scheme shows a sum rate close to that of the ‘**MMSE**’ scheme,

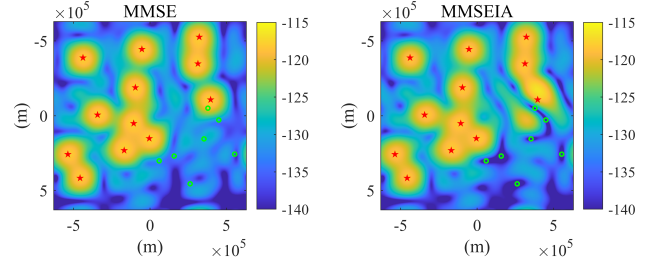


Fig. 4. Satellite beam patterns (red stars represent satellite UTs and green circles represent terrestrial UTs), $I_{\text{thr}} = -150$ dBW, $\text{SNR} = 10$ dB.

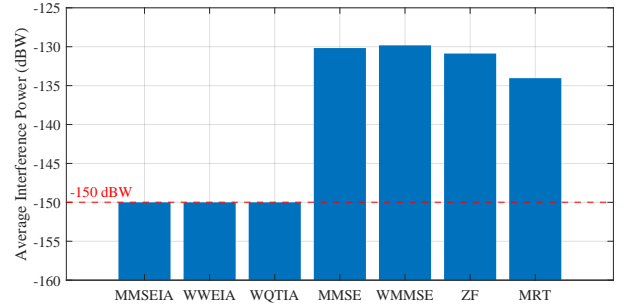


Fig. 5. Average interference power, $\text{SNR} = 10$ dB.

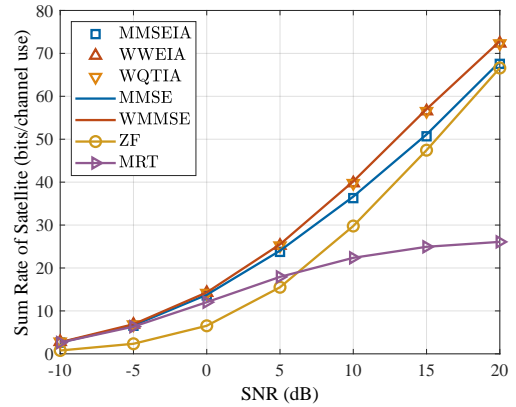


Fig. 6. Satellite sum rate vs SNR, $I_{\text{thr}} = -150$ dBW.

indicating its effectiveness in sustaining capacity. Furthermore, both the ‘**WWEIA**’ and ‘**WQTIA**’ schemes outperform ‘**MMSE**’ and closely approach the performance of ‘**WMMSE**’. These two iterative algorithms significantly enhance the sum rate, while the closed-form ‘**MMSEIA**’ operates with lower computational complexity.

For the iterative algorithms ‘**WWEIA**’ and ‘**WQTIA**’, we study their convergence behaviors in satellite sum rate. As illustrated in Fig. 7, the satellite sum rate performances of the proposed schemes ‘**WWEIA**’ and ‘**WQTIA**’ quickly converge within the specified number of iterations. The results are verified at $\text{SNR} = 0$ dB, $\text{SNR} = 10$ dB, and $\text{SNR} = 20$ dB,

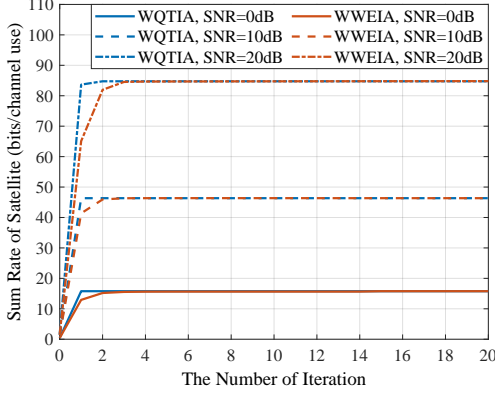
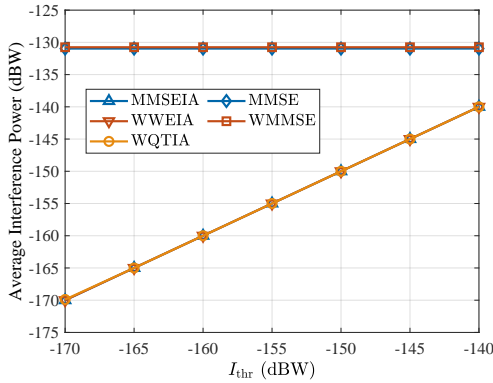
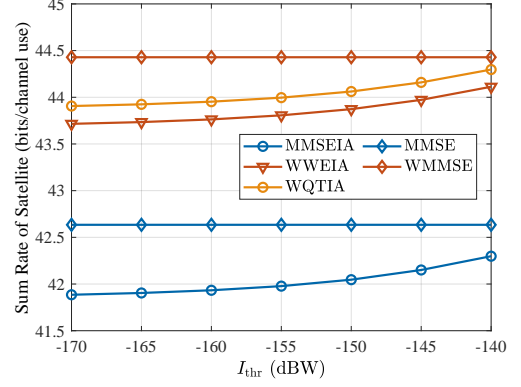
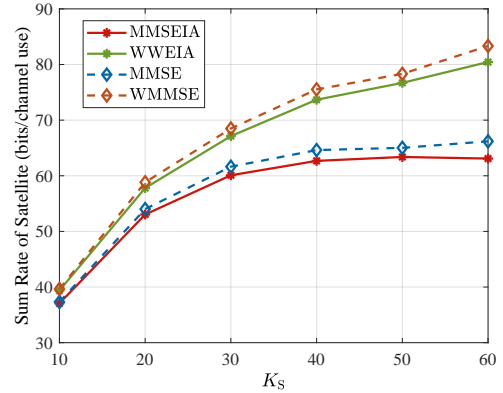


Fig. 7. The convergence of satellite sum rate.

Fig. 8. Average interference vs I_{thr} , SNR = 10 dB.Fig. 9. Satellite sum rate vs I_{thr} , SNR = 10 dB.Fig. 10. Satellite sum rate vs K_S , $I_{\text{thr}} = -150$ dBW, SNR = 10 dB.

demonstrating consistent convergenc performance. We also observe that ‘WWEIA’ takes more iterations to converge as SNR increases.

B. Effect of Interference Thresholds and Satellite UT Numbers

Fig. 8 and Fig. 9 illustrate the impact of interference thresholds on the satellite sum rate and average interference power performance. As illustrated in Fig. 8, the average interference power remains the same with ‘MMSE’ and ‘WMMSE’ schemes, but decreases adaptively as the interference threshold I_{thr} is reduced with ‘MMSEIA’, ‘WWEIA’, and ‘WQTIA’ schemes. As shown in Fig. 9, when we set the SNR as 10 dB, the sum rate for the ‘MMSE’ and ‘WMMSE’ schemes remains unchanged. However, the satellite sum rate for both the ‘MMSEIA’ and ‘WWEIA’ schemes decreases slightly as the interference threshold I_{thr} is reduced. Specifically, when $I_{\text{thr}} = -170$ dBW, all three TX beamforming algorithms exhibit a sum rate reduction of approximately 1 % compared to the case when $I_{\text{thr}} = -140$ dBW.

Furthermore, we study the impact of different satellite UT numbers on the proposed TX beamforming schemes, with a fixed number of terrestrial BSs and a fixed number of terrestrial UTs. Taking the lower-complexity ‘MMSEIA’ and ‘WWEIA’ as examples, it can be observed in Fig. 10 that the sum rate of the satellite increases with the number of satellite UTs K_S . However, the rate of increase diminishes

as K_S grows, and when $K_S \geq 40$, the sum rate of ‘MMSEIA’ approaches a plateau, remaining nearly constant thereafter. Notably, the satellite sum rate performance of ‘MMSEIA’ approaches that of ‘MMSE’, and ‘WWEIA’ approaches the performance of ‘WMMSE’.

C. Validation of Position-Aided Interference Approximation

In this subsection, we further validate the performance after interference approximation in beamforming design. The integral-form interference channel term $\Upsilon_{\text{sg}}^{\text{int}}$ is approximated by the corresponding satellite-to-terrestrial BS channels, denoted as Υ_{sg} . We fix the terrestrial BS radius at $R_{\text{bs}} = 500$ m and compare the performance of the approximated schemes ‘MMSEIA-PA’, ‘WWEIA-PA’, and ‘WQTIA-PA’ with the original TX beamforming schemes ‘MMSEIA’, ‘WWEIA’, and ‘WQTIA’.

In Fig. 11, the results reveal that all three PA schemes nearly meet the interference threshold of -150 dBW at 10 dB, representing the effectiveness of the approximation in terms of interference management. In Fig. 12, the sum rate performance of the approximated schemes is consistent with that of the original schemes. The proposed PA method reduces computational complexity while maintaining effective interference management and high satellite sum rate performance, highlighting the practical benefits of PA schemes in ITSN systems.

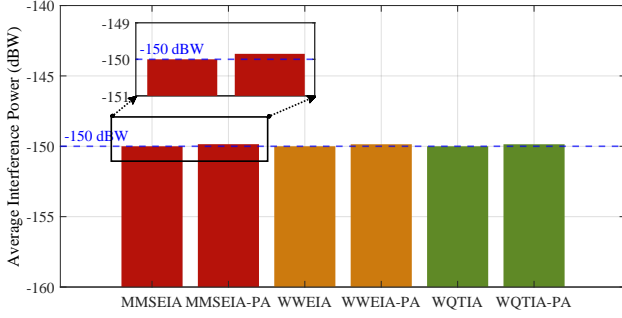


Fig. 11. Average interference power, $I_{\text{thr}} = -150$ dBW, SNR = 10 dB.

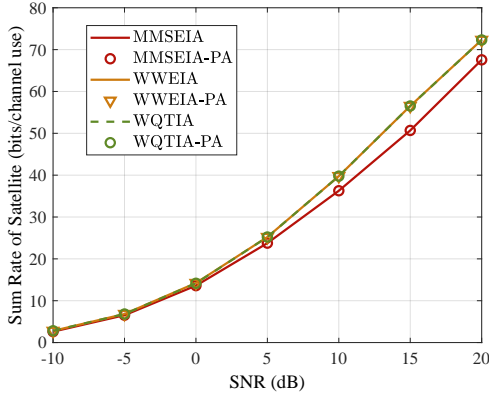


Fig. 12. Satellite sum rate vs SNR, $I_{\text{thr}} = -150$ dBW.

TABLE II
COMPLEXITY COMPARISON

Scheme	Complexity Order
WQTIA	$\mathcal{O}(N_A (T_A (M_S^3 K_S^3) + M_S^2 N_G N_r N_\phi))$
WWEIA	$\mathcal{O}(N_B (T_B + M_S^2 K_S + M_S^2 N_G N_r N_\phi + M_S^3))$
MMSEIA	$\mathcal{O}(M_S^2 N_G N_r N_\phi + M_S^3)$
WQTIA-PA	$\mathcal{O}(N_A (T_A (M_S^3 K_S^3) + M_S^2 N_G))$
WWEIA-PA	$\mathcal{O}(N_B (T_B + M_S^2 K_S^2 + M_S^2 N_G + M_S^3))$
MMSEIA-PA	$\mathcal{O}(M_S^2 N_G + M_S^3)$

D. Comparison of Computational Complexity

In this subsection, we compare the order of computational complexity of the schemes considered in Tab. II. Here, N_A and N_B represent the number of outer loop iterations of ‘WQTIA’ and ‘WWEIA’, respectively. From this comparison, we can conclude that ‘WWEIA’ significantly reduces the complexity compared to ‘WQTIA’, primarily due to its more efficient iterative procedures. The closed-form solution, ‘MMSEIA’, exhibits a lower complexity than both ‘WQTIA’ and ‘WWEIA’. Furthermore, PA schemes reduce the complexity by decreasing the dimension from the number of discrete samples $N_G N_r N_\phi$ to the number of terrestrial BSs N_G .

VII. CONCLUSION

This paper investigated robust TX beamforming based on sCSI, mitigating satellite-to-terrestrial UT interference in IT-SNs. We established an integral-form interference model free of shared CSI and designed robust TX beamforming schemes

under the power budget and the interference threshold. The WSR problem was iteratively solved after MCQT, while an equivalent WMMSE framework achieved a lower-complexity iterative optimization. Furthermore, we derived a closed-form solution for the MMSE criterion and applied a bisection method to meet the interference threshold. To reduce reliance on complex integral calculations, we proposed an approximation scheme based on terrestrial BS positions. Simulation results showed the level of interference mitigation that can be achieved with the proposed schemes and verified the effectiveness of the PA schemes, allowing efficient spectrum sharing. In future work, we will extend these schemes to satellite uplinks and terrestrial BS transmission within the ITSN framework.

APPENDIX A PROOF OF PROPOSITION 1

We substitute $\mathbf{h}_{ss,k}$ with $\mathbf{b}_k = e^{-j\psi_k} \mathbf{h}_{ss,k}$ and $\psi_k = 2\pi(t\nu_k^{\text{sat}} - f\tau_k^{\text{min}})$ in the sum rate of the satellite system as follows

$$\begin{aligned}
 & \sum_{k=1}^{K_S} \mathbb{E}_{\mathbf{H}_{ss}} \left\{ a_k \log_2 \left(1 + \frac{\mathbf{p}_k^H \mathbf{h}_{ss,k} \mathbf{h}_{ss,k}^H \mathbf{p}_k}{\sum_{i \neq k} \mathbf{p}_i^H \mathbf{h}_{ss,k} \mathbf{h}_{ss,k}^H \mathbf{p}_i + \sigma_k^2} \right) \right\} \\
 &= \sum_{k=1}^{K_S} \mathbb{E}_{\mathbf{B}} \left\{ a_k \log_2 \left(1 + \frac{\mathbf{p}_k^H e^{j\psi_k} \mathbf{b}_k e^{-j\psi_k} \mathbf{b}_k^H \mathbf{p}_k}{\sum_{i \neq k} \mathbf{p}_i^H e^{j\psi_k} \mathbf{b}_k e^{-j\psi_k} \mathbf{b}_k^H \mathbf{p}_i + \sigma_k^2} \right) \right\} \\
 &= \sum_{k=1}^{K_S} \mathbb{E}_{\mathbf{B}} \left\{ a_k \log_2 \left(1 + \frac{\mathbf{p}_k^H \mathbf{b}_k \mathbf{b}_k^H \mathbf{p}_k}{\sum_{i \neq k} \mathbf{p}_i^H \mathbf{b}_k \mathbf{b}_k^H \mathbf{p}_i + \sigma_k^2} \right) \right\}. \tag{44}
 \end{aligned}$$

This completes the proof.

APPENDIX B PROOF OF PROPOSITION 2

The Lagrangian function is derived as

$$\begin{aligned}
 \mathcal{L}(\mathbf{P}, \beta, \lambda) &= \frac{\text{Tr}\{\mathbf{P}^H \mathbf{\Upsilon}_{ss} \mathbf{P}\}}{\beta^2} - \frac{\text{Tr}\{\bar{\mathbf{H}}_{ss} \mathbf{P}\}}{\beta} - \frac{\text{Tr}\{\mathbf{P}^H \bar{\mathbf{H}}_{ss}\}}{\beta} \\
 &+ K_S + \frac{K_S \sigma_s^2}{\beta^2} + \frac{\varsigma}{\beta^2} \text{Tr}\{\mathbf{P}^H \mathbf{\Upsilon}_{sg} \mathbf{P}\} + \lambda (\text{Tr}\{\mathbf{P} \mathbf{P}^H\} - P_T). \tag{45}
 \end{aligned}$$

Then, we set the gradient of the Lagrangian function to zero

$$\nabla_{\mathbf{P}} \mathcal{L} = \frac{\mathbf{\Upsilon}_{ss} \mathbf{P}}{\beta^2} - \frac{\bar{\mathbf{H}}_{ss}}{\beta} + \frac{\varsigma}{\beta^2} \mathbf{\Upsilon}_{sg} \mathbf{P} + \lambda \mathbf{P} = \mathbf{0}, \tag{46}$$

and we obtain

$$\mathbf{P} = \beta (\mathbf{\Upsilon}_{ss} + \varsigma \mathbf{\Upsilon}_{sg} + \lambda \beta^2 \mathbf{I})^{-1} \bar{\mathbf{H}}_{ss}. \tag{47}$$

We define $\zeta = \lambda \beta^2$, $\mathbf{A} = \mathbf{\Upsilon}_{ss} + \varsigma \mathbf{\Upsilon}_{sg} + \zeta \mathbf{I}$, $\mathbf{P} = \beta \mathbf{A}^{-1} \bar{\mathbf{H}}_{ss}$ and $\tilde{\mathbf{\Upsilon}}_{ss} = \bar{\mathbf{H}}_{ss} \bar{\mathbf{H}}_{ss}^H$. Through normalization, we have $\beta = \sqrt{\frac{P_T}{\text{Tr}\{\mathbf{A}^{-2} \tilde{\mathbf{\Upsilon}}_{ss}\}}}$, and the problem is transformed into an unconstrained optimization problem: $\min_{\zeta} f(\mathbf{P}(\zeta), \beta(\zeta))$, where the objective function is

$$\begin{aligned}
 f(\zeta) &= \text{Tr}\{\mathbf{A}^{-1} \mathbf{\Upsilon}_{ss} \mathbf{A}^{-1} \tilde{\mathbf{\Upsilon}}_{ss}\} - 2 \text{Tr}\{\mathbf{A}^{-1} \tilde{\mathbf{\Upsilon}}_{ss}\} + K_S \\
 &+ \frac{K_S \sigma_s^2}{P_T} \text{Tr}\{\mathbf{A}^{-2} \tilde{\mathbf{\Upsilon}}_{ss}\} + \varsigma \text{Tr}\{\mathbf{\Upsilon}_{sg} \mathbf{A}^{-1} \tilde{\mathbf{\Upsilon}}_{ss} \mathbf{A}^{-1}\}. \tag{48}
 \end{aligned}$$

We calculate the gradient of (45) with respect to ζ as $\nabla_{\zeta} f = 2 \text{Tr} \left\{ \left(\zeta - \frac{K_S \sigma_s^2}{P_T} \right) (\mathbf{A}^{-3} \tilde{\mathbf{Y}}_{ss}) \right\}$, and set it to zero. Therefore, we have $\zeta = \lambda \beta^2 = \frac{K_S \sigma_s^2}{P_T}$. Substituting this into \mathbf{P} and β gives the closed-form solution

$$\mathbf{P}^* = \beta^* \left(\mathbf{Y}_{ss} + \zeta \mathbf{Y}_{sg} + \frac{K_S \sigma_s^2}{P_T} \mathbf{I} \right)^{-1} \bar{\mathbf{H}}_{ss}, \quad (49)$$

$$\beta^* = \sqrt{\frac{P_T}{\left\| \left(\mathbf{Y}_{ss} + \zeta \mathbf{Y}_{sg} + \frac{K_S \sigma_s^2}{P_T} \mathbf{I} \right)^{-1} \bar{\mathbf{H}}_{ss} \right\|_F^2}}. \quad (50)$$

This completes the proof.

APPENDIX C

PROOF OF PROPOSITION 3

From (33) and (35), we simplify $\mathbf{P}(\zeta) = \beta \mathbf{A}^{-1} \bar{\mathbf{H}}_{ss}$, $\alpha = \text{Tr} \{ \mathbf{A}^{-2} \tilde{\mathbf{Y}}_{ss} \}$ and $\tilde{\mathbf{Y}}_{ss} = \bar{\mathbf{H}}_{ss} \bar{\mathbf{H}}_{ss}^H$. The gradient can be derived as

$$\nabla_{\zeta} I_{sg} = \frac{2\beta^2}{\alpha} \text{Tr} \left\{ \tilde{\mathbf{Y}}_{ss} \mathbf{A}^{-1} \mathbf{Y}_{sg}^{\text{int}} \mathbf{A}^{-2} (\mathbf{A}^{-1} \mathbf{Y}_{sg}^{\text{int}} \tilde{\mathbf{Y}}_{ss} \mathbf{A}^{-1} - \alpha \mathbf{Y}_{sg}^{\text{int}}) \right\}, \quad (51)$$

where both the complex matrix $\mathbf{M} = \frac{2\beta^2}{\alpha} \tilde{\mathbf{Y}}_{ss} \mathbf{A}^{-1} \mathbf{Y}_{sg}^{\text{int}} \mathbf{A}^{-2}$ and matrix $\mathbf{N} = \mathbf{A}^{-1} \mathbf{Y}_{sg}^{\text{int}} \tilde{\mathbf{Y}}_{ss} \mathbf{A}^{-1} - \alpha \mathbf{Y}_{sg}^{\text{int}}$ are Hermitian matrices. From *Von Neumann Trace Inequality*, we derive that

$$\text{Tr} \{ \mathbf{M} \mathbf{N} \} = \sum_{i=1}^{M_S} \lambda_i(\mathbf{M} \mathbf{N}) \leq \sum_{i=1}^{M_S} \lambda_i(\mathbf{M}) \lambda_i(\mathbf{N}), \quad (52)$$

where $\lambda_i(\cdot)$ denotes the eigenvalues. They are arranged in descending order such that $\lambda_1(\mathbf{M}) \geq \lambda_2(\mathbf{M}) \geq \dots \geq \lambda_{M_S}(\mathbf{M})$ and $\lambda_1(\mathbf{N}) \geq \lambda_2(\mathbf{N}) \geq \dots \geq \lambda_{M_S}(\mathbf{N})$. From the *Cauchy-Buniakowsky-Schwarz Inequality*,

$$\begin{aligned} \sum_{i=1}^{M_S} \lambda_i(\mathbf{M}) \lambda_j(\mathbf{N}) &\leq \sqrt{\left[\sum_{i=1}^{M_S} \lambda_i(\mathbf{M})^2 \right] \left[\sum_{j=1}^{M_S} \lambda_j(\mathbf{N})^2 \right]} \\ &\leq \left[\sum_{i=1}^{M_S} \lambda_i(\mathbf{M}) \right] \left[\sum_{j=1}^{M_S} \lambda_j(\mathbf{N}) \right] = \text{Tr} \{ \mathbf{M} \} \text{Tr} \{ \mathbf{N} \}, \end{aligned} \quad (53)$$

i.e., $\text{Tr} \{ \mathbf{M} \mathbf{N} \} \leq \text{Tr} \{ \mathbf{M} \} \text{Tr} \{ \mathbf{N} \}$. Similarly, we define $\mathbf{T} = \tilde{\mathbf{Y}}_{ss} \mathbf{A}^{-2} - \alpha$ and $\mathbf{S} = \mathbf{Y}_{sg}^{\text{int}}$ and we have $\text{Tr} \{ \mathbf{T} \mathbf{S} \} \leq \text{Tr} \{ \mathbf{T} \} \text{Tr} \{ \mathbf{S} \}$. Substituting these inequalities into (51),

$$\begin{aligned} \nabla_{\zeta} I_{sg} &\leq \text{Tr} \left\{ \frac{2\beta^2}{\alpha} \tilde{\mathbf{Y}}_{ss} \mathbf{A}^{-1} \mathbf{Y}_{sg}^{\text{int}} \mathbf{A}^{-2} \right\} \\ &\quad \times \text{Tr} \left\{ \mathbf{A}^{-1} \mathbf{Y}_{sg}^{\text{int}} \tilde{\mathbf{Y}}_{ss} \mathbf{A}^{-1} - \alpha \mathbf{Y}_{sg}^{\text{int}} \right\} \leq 0. \end{aligned} \quad (54)$$

This concludes the proof.

REFERENCES

- [1] L. Kuang, X. Chen, C. Jiang, H. Zhang, and S. Wu, "Radio resource management in future terrestrial-satellite communication networks," *IEEE Wirel. Commun.*, vol. 24, no. 5, pp. 81–87, Oct. 2017.
- [2] A. I. Perez-Neira, M. A. Vazquez, M. B. Shankar, S. Maleki, and S. Chatzinotas, "Signal processing for high-throughput satellites: Challenges in new interference-limited scenarios," *IEEE Signal Process. Mag.*, vol. 36, no. 4, pp. 112–131, Jul. 2019.
- [3] G. Hattab, P. Moorut, E. Visotsky, M. Cudak, and A. Ghosh, "Interference analysis of the coexistence of 5G cellular networks with satellite earth stations in 3.7–4.2GHz," in *Proc. IEEE Int. Conf. Commun. Workshops (ICC Workshops)*, Jul. 2018, pp. 1–6.
- [4] V. Deslandes, J. Tronc, and A.-L. Beylot, "Analysis of interference issues in integrated satellite and terrestrial mobile systems," in *Proc. Adv. Satell. Multimedia Syst. Conf. Signal Process. Space Commun. Workshop (ASMS/SPSC)*, 2010, pp. 256–261.
- [5] M. Jia, X. Gu, Q. Guo, W. Xiang, and N. Zhang, "Broadband hybrid satellite-terrestrial communication systems based on cognitive radio toward 5G," *IEEE Wirel. Commun.*, vol. 23, no. 6, pp. 96–106, Dec. 2016.
- [6] E. Lagunas, C. G. Tsinos, S. K. Sharma, and S. Chatzinotas, "5G cellular and fixed satellite service spectrum coexistence in C-band," *IEEE Access*, vol. 8, pp. 72 078–72 094, 2020.
- [7] X. Fang, W. Feng, T. Wei, Y. Chen, N. Ge, and C.-X. Wang, "5G embraces satellites for 6G ubiquitous IoT: Basic models for integrated satellite terrestrial networks," *IEEE Internet Things J.*, vol. 8, no. 18, pp. 14 399–14 417, Sep. 2021.
- [8] D. Peng, A. Bandi, Y. Li, S. Chatzinotas, and B. Ottersten, "Hybrid beamforming, user scheduling, and resource allocation for integrated terrestrial-satellite communication," *IEEE Trans. Veh. Technol.*, vol. 70, no. 9, pp. 8868–8882, Sep. 2021.
- [9] H. Nguyen-Kha, V. Nguyen Ha, E. Lagunas, S. Chatzinotas, and J. Grotz, "Joint two-tier user association and resource management for integrated satellite-terrestrial networks," *IEEE Trans. Wireless Commun.*, vol. 23, no. 11, pp. 16 648–16 665, Nov. 2024.
- [10] H.-W. Lee, C.-C. Chen, C.-I. S. Liao, A. Medles, D. Lin, I.-K. Fu, and H.-Y. Wei, "Interference mitigation for reverse spectrum sharing in B5G/6G satellite-terrestrial networks," *IEEE Trans. Veh. Technol.*, vol. 73, no. 3, pp. 4247–4263, Mar. 2024.
- [11] D. Peng, D. He, Y. Li, and Z. Wang, "Integrating terrestrial and satellite multibeam systems toward 6G: Techniques and challenges for interference mitigation," *IEEE Wirel. Commun.*, vol. 29, no. 1, pp. 24–31, Feb. 2022.
- [12] T. Wei, W. Feng, Y. Chen, C.-X. Wang, N. Ge, and J. Lu, "Hybrid satellite-terrestrial communication networks for the maritime internet of things: Key technologies, opportunities, and challenges," *IEEE Internet Things J.*, vol. 8, no. 11, pp. 8910–8934, Jun. 2021.
- [13] E. Lagunas, S. K. Sharma, S. Maleki, S. Chatzinotas, and B. Ottersten, "Resource allocation for cognitive satellite communications with incumbent terrestrial networks," *IEEE Trans. Cogn. Commun. Netw.*, vol. 1, no. 3, pp. 305–317, Sep. 2015.
- [14] Lagunas, Eva and Sharma, Shree Krishna and Maleki, Sina and Chatzinotas, Symeon and Ottersten, Bjorn, "Power control for satellite uplink and terrestrial fixed-service co-existence in Ka-band," in *Proc. IEEE Veh. Technol. Conf. (VTC2015-Fall)*, Sep. 2015, pp. 1–5.
- [15] G. Ziaragkas, G. Poziopoulou, J. Nez-Martnez, J. Baranda, I. Moreno, C. Tsinos, S. Maleki, S. K. Sharma, M. Alodeh, and S. Chatzinotas, "SANSaHybrid terrestrialsatellite backhaul network: scenarios, use cases, KPIs, architecture, network and physical layer techniques," *Int. J. Satell. Commun. Networking*, vol. 35, no. 5, pp. 379–405, Oct. 2017.
- [16] E. Lagunas, S. Maleki, L. Lei, C. Tsinos, S. Chatzinotas, and B. Ottersten, "Carrier allocation for hybrid satellite-terrestrial backhaul networks," in *IEEE Int. Conf. Commun. Workshops (ICC Workshops)*, Jun. 2017, pp. 718–723.
- [17] C. Jiang, X. Zhu, L. Kuang, Y. Qian, and J. Lu, "Multimedia multicast beamforming in integrated terrestrial-satellite networks," in *IEEE Int. Wirel. Commun. Mob. Comput. Conf., (IWCMC)*, Jun. 2017, pp. 340–345.
- [18] H. Baek and J. Lim, "Spectrum sharing for coexistence of fixed satellite services and frequency hopping tactical data link," *IEEE J. Sel. Areas Commun.*, vol. 34, no. 10, pp. 2642–2649, Oct. 2016.
- [19] K. An, M. Lin, W.-P. Zhu, Y. Huang, and G. Zheng, "Outage performance of cognitive hybrid satellite-terrestrial networks with interference constraint," *IEEE Trans. Veh. Technol.*, vol. 65, no. 11, pp. 9397–9404, Nov. 2016.
- [20] L. You, K.-X. Li, J. Wang, X. Gao, X.-G. Xia, and B. Ottersten, "Massive MIMO transmission for LEO satellite communications," *IEEE J. Sel. Areas Commun.*, vol. 38, no. 8, pp. 1851–1865, Aug. 2020.
- [21] A. Pastukh, V. Tikhvinskiy, S. S. Dymkova, and O. V. Varlamov, "Challenges of using the L-band and S-band for direct-to-cellular satellite 5G-6G NTN systems," *Technologies*, 2023.
- [22] J. Heo, S. Sung, H. Lee, I. Hwang, and D. Hong, "MIMO satellite communication systems: A survey from the PHY layer perspective," *IEEE Commun. Surv. Tutor.*, vol. 25, no. 3, pp. 1543–1570, 2023.
- [23] V. Joroughi, M. V. Vazquez, A. I. Prez-Neira, and B. Devillers, "Onboard beam generation for multibeam satellite systems," *IEEE Trans. Wireless Commun.*, vol. 16, no. 6, pp. 3714–3726, Jun. 2017.

- [24] M. Khammassi, A. Kammoun, and M.-S. Alouini, "Precoding for high-throughput satellite communication systems: A survey," *IEEE Commun. Surv. Tutor.*, vol. 26, no. 1, pp. 80–118, 2024.
- [25] G. Geraci, D. Lopez-Perez, M. Benzaghta, and S. Chatzinotas, "Integrating terrestrial and non-terrestrial networks: 3D opportunities and challenges," *IEEE Commun. Mag.*, vol. 61, no. 4, pp. 42–48, Apr. 2023.
- [26] K. Ntontin, E. Lagunas, J. Querol, J. u. Rehman, J. Grotz, S. Chatzinotas, and B. Ottersten, "A vision, survey, and roadmap toward space communications in the 6G and beyond era," *Proc. IEEE*, pp. 1–37, 2025.
- [27] D. Tuzi, T. Delamotte, and A. Knopp, "Satellite swarm-based antenna arrays for 6G direct-to-cell connectivity," *IEEE Access*, vol. 11, pp. 36 907–36 928, 2023.
- [28] T. Yoo and A. Goldsmith, "Optimality of zero-forcing beamforming with multiuser diversity," in *Proc. IEEE Int. Conf. Commun. (ICC)*, vol. 1, May 2005, pp. 542–546.
- [29] C. Peel, B. Hochwald, and A. Swindlehurst, "A vector-perturbation technique for near-capacity multi-antenna multiuser communication-part I: Channel inversion and regularization," *IEEE Trans. Commun.*, vol. 53, no. 1, pp. 195–202, Jan. 2005.
- [30] S. S. Christensen, R. Agarwal, E. De Carvalho, and J. M. Cioffi, "Weighted sum-rate maximization using weighted MMSE for MIMO-BC beamforming design," *IEEE Trans. Wireless Commun.*, vol. 7, no. 12, pp. 4792–4799, Dec. 2008.
- [31] Y. Wang, H. Hou, X. Yi, W. Wang, and S. Jin, "Towards unified AI models for MU-MIMO communications: A tensor equivariance framework," *arXiv preprint arXiv:2406.09022*, 2024. [Online]. Available: <https://arxiv.org/abs/2406.09022>
- [32] S. Wu, Y. Wang, G. Sun, L. You, W. Wang, and R. Ding, "Energy and computational efficient precoding for LEO satellite communications," in *Proc. IEEE Glob. Commun. Conf (GLOBECOM)*, Dec. 2023, pp. 1872–1877.
- [33] E. Björnson, M. Bengtsson, and B. Ottersten, "Optimal multiuser transmit beamforming: A difficult problem with a simple solution structure," *IEEE Signal Process. Mag.*, vol. 31, no. 4, pp. 142–148, Jul. 2014.
- [34] Y. Liu, Y. Wang, J. Wang, L. You, W. Wang, and X. Gao, "Robust downlink precoding for LEO satellite systems with per-antenna power constraints," *IEEE Trans. Veh. Technol.*, vol. 71, no. 10, pp. 10694–10711, Oct. 2022.
- [35] H. Dong, C. Hua, L. Liu, W. Xu, S. Guo, and R. Tafazolli, "Joint beamformer design and user scheduling for integrated terrestrial-satellite networks," *IEEE Trans. Wireless Commun.*, vol. 22, no. 10, pp. 6398–6414, Oct. 2023.
- [36] Y. Jiang, J. Ouyang, C. Yin, Z. Xu, X. Tao, and L. Lou, "Downlink beamforming scheme for hybrid satellite-terrestrial networks," *IET Commun.*, vol. 12, no. 18, p. 23422346, Oct. 2018.
- [37] S. K. Sharma, S. Chatzinotas, and B. Ottersten, "Transmit beamforming for spectral coexistence of satellite and terrestrial networks," in *Proc. IEEE Int. Conf. Cognitive Radio Oriented Wirel. Networks Commun., (CROWNCOM)*, Jul. 2013, pp. 275–281.
- [38] Q. Wang, H. Zhang, J.-B. Wang, F. Yang, and G. Y. Li, "Joint beamforming for integrated mmwave satellite-terrestrial self-backhauled networks," *IEEE Trans. Veh. Technol.*, vol. 70, no. 9, pp. 9103–9117, Sep. 2021.
- [39] Y. Zhang, L. Yin, C. Jiang, and Y. Qian, "Joint beamforming design and resource allocation for terrestrial-satellite cooperation system," *IEEE Trans. Commun.*, vol. 68, no. 2, pp. 778–791, Feb. 2020.
- [40] H. Zhang, C. Jiang, J. Wang, L. Wang, Y. Ren, and L. Hanzo, "Multicast beamforming optimization in cloud-based heterogeneous terrestrial and satellite networks," *IEEE Trans. Veh. Technol.*, vol. 69, no. 2, pp. 1766–1776, Feb. 2020.
- [41] C. Liu, W. Feng, Y. Chen, C.-X. Wang, and N. Ge, "Optimal beamforming for hybrid satellite terrestrial networks with nonlinear PA and imperfect CSIT," *IEEE Wireless Commun. Lett.*, vol. 9, no. 3, pp. 276–280, Mar. 2020.
- [42] M. A. Vazquez, L. Blanco, and A. I. Prez-Neira, "Hybrid analog digital transmit beamforming for spectrum sharing backhaul networks," *IEEE Trans. Signal Process.*, vol. 66, no. 9, pp. 2273–2285, May 2018.
- [43] X. Zhu, C. Jiang, L. Yin, L. Kuang, N. Ge, and J. Lu, "Cooperative multigroup multicast transmission in integrated terrestrial-satellite networks," *IEEE J. Sel. Areas Commun.*, vol. 36, no. 5, pp. 981–992, May 2018.
- [44] D. Kim, S. Cho, W. Shin, J. Park, and D. K. Kim, "Distributed precoding for satellite-terrestrial integrated networks without sharing CSIT: A rate-splitting approach," *IEEE Trans. Wireless Commun.*, 2025.
- [45] 3GPP, "Study on new radio (NR) to support non-terrestrial networks," 3rd Generation Partnership Project, Tech. Rep. TR 38.811, Sep. 2020.
- [46] S. Wu, G. Sun, Y. Wang, L. You, W. Wang, and R. Ding, "Low-complexity user scheduling for LEO satellite communications," *IET Commun.*, vol. 17, no. 12, pp. 1368–1383, May 2023.
- [47] C. Wu, X. Yi, Y. Zhu, W. Wang, L. You, and X. Gao, "Channel prediction in high-mobility massive MIMO: From spatio-temporal autoregression to deep learning," *IEEE J. Sel. Areas Commun.*, vol. 39, no. 7, pp. 1915–1930, Jul. 2021.
- [48] N. Letzepis and A. J. Grant, "Capacity of the multiple spot beam satellite channel with rician fading," *IEEE Trans. Inf. Theory*, vol. 54, no. 11, pp. 5210–5222, Nov. 2008.
- [49] 3GPP, "Solutions for NR to support non-terrestrial networks (NTN): Non-terrestrial networks (NTN) related RF and co-existence aspects," 3rd Generation Partnership Project, Tech. Rep. TR 38.863, Mar. 2025.
- [50] Federal Communications Commission (FCC), "Satellite Space Stations: Application to Launch and Operate," FCC report. <https://fcc.report/IBFS/Filing-List/SAT-LOA> (accessed: Apr. 17, 2025).
- [51] W. Wang, Y. Tong, L. Li, A.-A. Lu, L. You, and X. Gao, "Near optimal timing and frequency offset estimation for 5G integrated LEO satellite communication system," *IEEE Access*, vol. 7, pp. 113 298–113 310, 2019.
- [52] J. Shi, A.-A. Lu, W. Zhong, X. Gao, and G. Y. Li, "Robust WMMSE precoder with deep learning design for massive MIMO," *IEEE Trans. Commun.*, vol. 71, no. 7, pp. 3963–3976, Jul. 2023.
- [53] K. Shen and W. Yu, "Fractional programming for communication systems part I: Power control and beamforming," *IEEE Trans. Signal Process.*, vol. 66, no. 10, pp. 2616–2630, May 2018.
- [54] M. Villalobos and Y. Zhang, "A trust-region interior-point method for nonlinear programming," in *TAPIA - Richard Tapia Celebr. Diversity Comput. Conf.*, Oct. 2005, pp. 7–9.
- [55] Z. Xiang, X. Gao, K.-X. Li, and X.-G. Xia, "Massive MIMO downlink transmission for multiple LEO satellite communication," *IEEE Trans. Commun.*, vol. 72, no. 6, pp. 3352–3364, Jun. 2024.
- [56] Q. Shi, M. Razaviyayn, Z.-Q. Luo, and C. He, "An iteratively weighted MMSE approach to distributed sum-utility maximization for a MIMO interfering broadcast channel," *IEEE Trans. Signal Process.*, vol. 59, no. 9, pp. 4331–4340, Sep. 2011.
- [57] K.-X. Li, X. Gao, and X.-G. Xia, "Channel estimation for LEO satellite massive MIMO OFDM communications," *IEEE Trans. Wireless Commun.*, vol. 22, no. 11, pp. 7537–7550, Nov. 2023.
- [58] H. Hou, Y. Wang, Y. Zhu, X. Yi, W. Wang, D. T. M. Slock, and S. Jin, "A tensor-structured approach to dynamic channel prediction for massive MIMO systems with temporal non-stationarity," *arXiv preprint arXiv:2412.06713*, 2024. [Online]. Available: <https://arxiv.org/abs/2412.06713>
- [59] K.-J. Wang and X. Zhang, "Penalty function-based precoding for downlink multiuser MIMO systems," *AEU Int. J. Electron. Commun.*, vol. 67, pp. 167–173, Feb. 2013.